RESEARCH ACTIVITIES VI
Department of Vacuum UV Photoscience

VI-A Electronic Structure and Decay Mechanism of Inner-Shell Excited Molecules

This project is being carried out in collaboration with Photon Factory (KEK-PF). We are interested in ionic fragmentations and electron emission via inner-shell excitation of molecules and in their polarization dependence. We have investigated vibronic couplings in the inner-shell excited states of some polyatomic molecules. Recently we have developed a new and simple method, the measurement of kinetic energy dependence of angle-resolved ion yields, to extend our approaches to other molecules. This method can be an alternative in comparison with mass-resolved techniques.

VI-A-1 Antisymmetric Stretching Vibrations in the O1s → 3$p\pi_u$ Rydberg Excited States of CO_2

Jun-ichi ADACHI, Nobuhiro KOSUGI, Eiji SHIGEMASA *(KEK-PF)* **and Akira YAGISHITA** *(KEK-PF)*

We have measured angle-resolved photoion-yield spectra (ARPIS) for the O1s excited states of CO_2 using linearly polarized synchrotron radiation. Vibrational structures with relatively large spacing (about 0.3 eV) are observed at about 538.4 eV in the I_{90} spectrum. These structures are assigned to the $\nu_3 = 0$, 1, and 2 levels (antisymmetric stretching mode) in the O1s → 3$p\pi_u$ Rydberg state. The dipole-allowed 1σ_g → 3$p\pi_u$ Rydberg state ($^1\Pi_u$) is coupled with the forbidden 1σ_u → 3$p\pi_u$ Rydberg state ($^1\Pi_g$) through the ν_3 (σ_u^+) mode excitation. On the other hand, the prominent O1s → 4$s\sigma_g$ peak is observed in the I_0 spectrum. The enhancement of the 4$s\sigma_g$ Rydberg state is attributed to the mixing with the O1s → 5σ_g* valence excited state.

References

1) A. Kivimäki, B. Kempgens, K. Maier, H. M. Köppe, M. N. Piancastelli, M Neeb, and A. M. Bradshaw, *Phys. Rev. Lett.* **79**, 998 (1997).
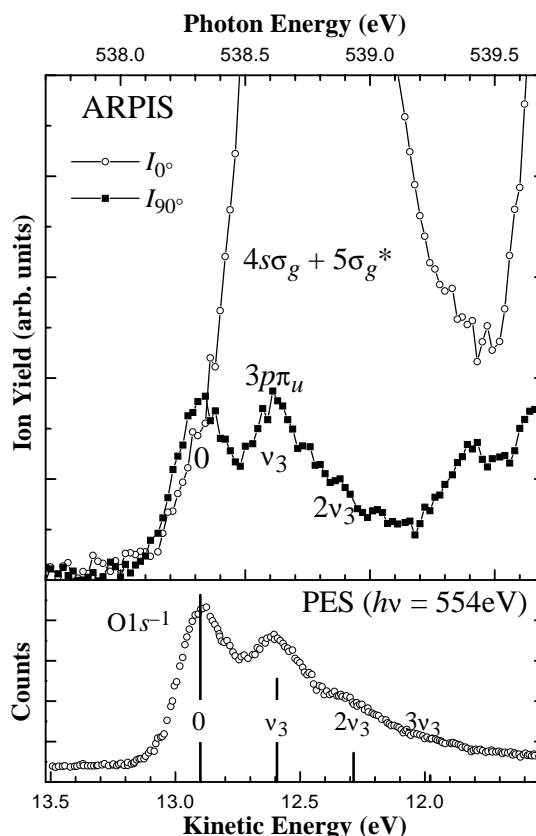
Figure 1. Angle-resolved ion-yield spectra for the O1s → 3$p\pi_u$ and 4$s\sigma_g$ Rydberg excited states of CO_2. The open circle (I_0) and square (I_{90}) show the ion yields in the 0° and 90° directions to the electric vector of the incident light, respectively. The O1s photoelectron spectrum of CO_2 obtained by Kivimäki *et al.*[1] is shown to compare with the present spectra.

VI-A-2 Renner-Teller Splitting in the C1s → π* Excited States of CS_2, OCS, and CO_2

Jun-ichi ADACHI, Nobuhiro KOSUGI, Eiji SHIGEMASA *(KEK-PF)* **and Akira YAGISHITA** *(KEK-PF)*

[*J. Chem. Phys.* **107**, 4919 (1997)]

Fragment ions energetically emitted following the perpendicular ($\Delta\Lambda = +1$) transitions of C1s → π* of

CS$_2$, OCS, and CO$_2$ are observed not only in the perpendicular (90°) direction but also in the parallel (0°) to the linear polarization; that is, ions have a momentum orthogonal to the linear molecule. This arises in the Renner-Teller (RT) vibronic coupling of bending vibrations in the C1s → in-plane π* excited state with a bent equilibrium geometry, though the RT splitting between C1s → out-of-plane π* excited state with a linear geometry and the C1s → in-plane π* state is not visible directly due to the lifetime broadening. The half-width at half-maximum on the lower energy side of the π* peak is sensitive to the RT splitting; 0.08, 0.11, and 0.29 eV for CS$_2$, OCS, and CO$_2$. The 0° ion yield is relatively small in CS$_2$ but is comparable to the 90° yield in CO$_2$; in the latter the peak maximum at 0° is 0.06 eV lower than at 90° and the anisotropy parameter β is heavily dependent on the photon energy. In CO$_2$ a great number of unresolved bending vibrations are coupled. In CS$_2$ the π* peak and β value are sharp and symmetric, indicating that the zero-point vibrational levels are only involved. In OCS three fine structures observed with separations of 0.21 eV are assigned to the ν$_3$ mode, which is comparable to the stretching mode in CO.

VI-A-3 Kinetic Energy Dependence of the Anisotropy Parameters for the Fragmentation of the C1s Excited States of C$_2$H$_4$

Jun-ichi ADACHI, Yasutaka TAKATA, Nobuhiro KOSUGI, Eiji SHIGEMASA *(KEK-PF)* **and Akira YAGISHITA** *(KEK-PF)*

We have measured angle-resolved ion-yield spectra for the C1s (1a_g and 1b_{3u}) excited states of C$_2$H$_4$ using linearly polarized synchrotron radiation. The anisotropy parameter for the fragment ions emitted following the C1s excitations of C$_2$H$_4$ is not directly related to the symmetry of the excited state because of some fragmentation patterns; the C-C bond and C-H bond breakings and other many-body fragmentations. However, it is found that the symmetries of valence and Rydberg states of C$_2$H$_4$ can be identified by measuring the kinetic energy dependence of the fragment ion yields. The relative H$^+$ yield to the other ion ones increases as the lower limit of the kinetic energy of the detected ions becomes higher. Then, the increasing, constant, and decreasing behaviors in the β$_R$ value with increasing the lower limit of the kinetic energy (R) indicate that the transitions are due to the 1a_g → b_{2u} /1b_{3u}→b_{1g}, 1a_g→b_{1u}/1b_{3u}→b_{2g}, and 1a_g → b_{3u} /1b_{3u} → a_g, respectively. The β$_R$ values for the C1s → 2b_{2u}* valence and 3pb_{1u} Rydberg transitions are almost constant within the bands. On the other hand, the β$_R$ values for the 4a_g* valence are changed just on the higher energy side. This result indicates that the peak at about 287.4 eV can be attributed to other electronic states or to vibronic states coupled in the bending or torsional mode.
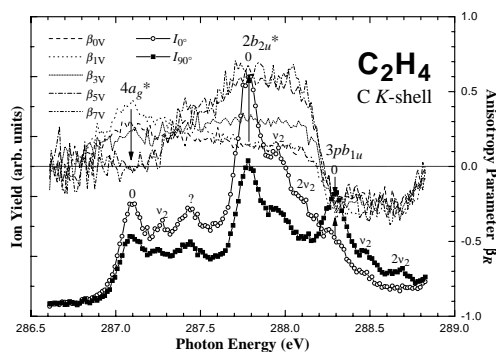
Figure 1. Angle-resolved ion-yield spectra with the larger kinetic energy than 3 eV for the C1s → Rydberg / σ* valence excited states of C$_2$H$_4$. The open circle (I_0) and square (I_{90}) show the ion yields in the 0° and 90° directions to the electric vector of the incident light, respectively. Various broken lines show the anisotropy parameter β$_R$ with R = 0, +1, +3, +5, and +7 eV.

VI-A-4 Kinetic Energy Dependence of Anisotropic Yields of Ionic Fragmentations Following S 1s Excitations of SO$_2$

Jun-ichi ADACHI, Yasutaka TAKATA, Nobuhiro KOSUGI, Eiji SHIGEMASA *(KEK-PF)*, **Akira YAGISHITA** *(KEK-PF)* **and Yoshinori KITAJIMA** *(KEK-PF)*

Several S 1s excited states of SO$_2$ are investigated in high-resolution angle-resolved ion-yield spectra using linearly polarized synchrotron radiation. The anisotropy parameter for the triatomic molecule is not directly related to the symmetry of the excited state due to the three-body fragmentation. The present work shows that the symmetries of the lowest three valence states and some low-lying Rydberg states are clearly identified by measuring the kinetic energy dependence of the fragment ion yields at two angles, where the oxygen ion yields are increased and the sulfur ion yields are decreased for the higher kinetic energy.

VI-A-5 Direct Determination of Partial Waves Contributions in the σ* Shape Resonance in CO Molecules

Eiji SHIGEMASA *(KEK-PF)*, **Jun-ichi ADACHI, Koichi SOEJIMA** *(Niigata Univ.)*, **Naoki WATANABE** *(Hokkaido Univ.)*, **Akira YAGISHITA** *(KEK-PF)* **and Nikolai A. CHEREPKOV** *(State Acad. Aerospace Instrum.)*

The first complete experiment for the C K-shell of CO molecules in the region of the σ* shape resonance has been performed by detecting photoelectrons in coincidence with fragment ions. Four ratios of dipole matrix elements and four phase shift differences have been extracted from the experimental data. Their analyses show that, in the σ* shape resonance due to the

ℓ mixing, d and f partial waves give the main contribution to the cross section, and f and g waves give the main contribution to a rapid increase of phase shift by .

VI-B Soft X-Ray Photoelectron-Photoabsorption Spectroscopy and Electronic Structure of Transition Metal Compounds

We have investigated electronic structures of molecular Ni complexes with planar structure by means of inner-shell photoabsorption and photoelectron spectra at the soft X-ray double crystal monochromator beamline BL1A of the UVSOR facility. Recently we have found that a one-electron picture is appropriate to interpret the Ni 2p photoabsorption and the resonant photoelectron spectra, and that the metal-to-ligand charge transfer (MLCT) is essential to describe the photoexcited states. This year we extended our study to Ni 1s and S 1s photoabsorption spectra, and also to other Ni compounds, to discuss intermolecular interaction and chemical bonds between metal and ligand.

VI-B-1 Metal-to-Ligand Charge Transfer Bands Observed in Polarized Ni 2*p* Photoabsorption Spectra of [Ni(mnt)$_2$]$^{2-}$

Takaki HATSUI *(Grad. Univ. Adv. Stud.)*, **Yasutaka TAKATA and Nobuhiro KOSUGI**

[*J. Electron Spectrosc. and Relat. Phenom.* submitted]

Linearly polarized Ni 2p photoabsorption spectra were measured for a planar Ni complex [(*n*-C$_4$H$_9$)$_4$N]$_2$-[Ni(mnt)$_2$] (mnt: 1,2-dicyanovinylene-1,2-dithiolato) as shown in Figure 1. The spectra show some characteristic bands above the strongest peak A. Because this complex has low-spin $3d^8$ configuration in the ground state, we expect intra-atomic transitions: strong one-electron transition to Ni $3d_{xy}$* and weak structure arising from intra-atomic correlation. Peak A is assigned to intra-atomic transition to Ni $3d_{xy}$*, which is confirmed by the observed polarization dependence of peak A. However, the polarization dependence shows that the characteristic bands B, C, and D can not be interepreted in terms of the correlation satellites. On the other hand, two mnt ligands produce two low-lying unoccupied orbitals L_{yz}* and L_{x2-y2}*, which may combine with Ni $3d_{yz}$ and Ni $3d_{x2-y2}$ orbitals, respectively. The polarization dependence shows that bands B and C are attributable to metal-to-ligand charge transfer (MLCT) transitions to L_{yz}* and L_{x2-y2}* in good agreement with ab initio molecular orbital predictions. Since stronger backbonding results in stronger MLCT bands, the in-plane backbonding ($3d_{x2-y2}$ L_{x2-y2}*) is as important as the out-of-plane one ($3d_{yz}$ L_{yz}*) in [Ni-(mnt)$_2$]$^{2-}$ complex.
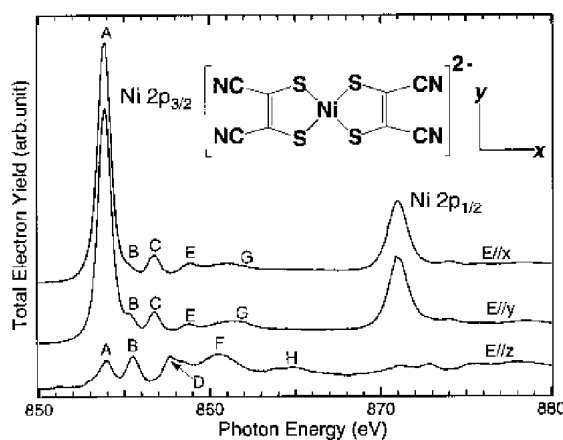
Figure 1. Polarized Ni 2p photoabsorption spectra of [(*n*-C$_4$H$_9$)N]$_2$[Ni(mnt)$_2$].

VI-B-2 Polarized Ni 1*s* and 2*p*, and S 1*s* Photo-absorption Spectra of [Ni(III)(mnt)$_2$]$^{1-}$

Takaki HATSUI *(Grad. Univ. Adv. Stud.)*, **Yasutaka TAKATA and Nobuhiro KOSUGI**

[*J. Synchrotron Rad.* submitted]

In formally trivalent Ni compounds with 1,2-dithiolates, the ligands are partially oxidized and the Ni metals have oxidation numbers between 2 and 3. In a molecular orbital picture, such compounds have a singly occupied molecular orbital (SOMO) which is delocalized over Ni and ligand. In order to characterize SOMO, polarized Ni 1s and 2p, and S 1s photo-absorption spectra have been measured for a formally trivalent Ni planar complex with local D_{2h} symmetry, [(C$_2$H$_5$)$_4$N][Ni(III)(mnt)$_2$] (mnt: dicyanovinylene-1,2-dithiolato). In the Ni 2p photoabsorption spectra (Figure 1), two strong peaks X and A are observed. The higher peak in energy is assigned to Ni 2p$_{3/2}$ Ni $3d_{xy}$* and the lower one to a transition to SOMO (coordinates were chosen as Figure 1 of VI-B-1 section). The polarization dependence shows that SOMO has the b_{2g} (d_{yz}) symmetry (out-of-plane *). Polarized S 1s photo-absorption spectra also show that the lowest transition (to SOMO) is of * character. These results indicate strongly delocalized character of the SOMO in the

formally trivalent Ni complex [Ni(mnt)$_2$]$^{1-}$.
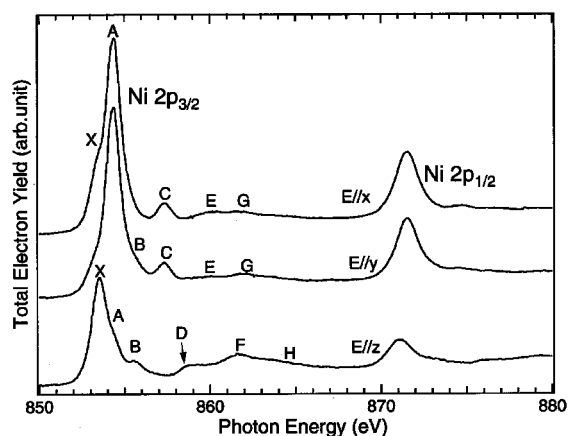
Figure 1. Polarized Ni $2p$ photoabsorption spectra of [(C$_2$H$_5$)$_4$N][Ni(mnt)$_2$].

VI-B-3 Strong Pre-Edge Peaks Found in Ni 1*s* Photoabsorption Spectra of Ni Planar Complexes

Takaki HATSUI *(Grad. Univ. Adv. Stud.)*, **Yasutaka TAKATA and Nobuhiro KOSUGI**

In order to obtain information on the low-lying unoccupied orbitals with p symmetry, we have measured linearly polarized Ni 1s photoabsorption spectra of bis(dimethylglyoximato)nickel(II) [Ni-(Hdmg)$_2$] and [(n-C$_4$H$_9$)$_4$N]$_2$[Ni(II)(mnt)$_2$] (mnt: 1,2-dicyanoethylene-1,2-dithiolato). These are planar complexes with D_{2h} symmetry and have low-spin 3d^8 configuration. The molecular structures and coordinates are shown in Figure 1 and inset of Figure 1 in VI-B-1. The Ni(Hdmg)$_2$ molecules are perpendicular to z axis and are rotated 90° around z axis. Therefore, the E $\perp$ z spectrum corresponds to an average of the E//x and E//y spectra, where E is the electric vector of incident photon. For [(n-C$_4$H$_9$)$_4$N]$_2$[Ni(II)(mnt)$_2$], all the [Ni(II)-(mnt)$_2$]$^{2-}$ anions are parallel to one another. Figure 1 shows the polarized Ni 1s photoabsorption spectra. For Ni(Hdmg)$_2$, the lowest weak band A is assigned to a quadruple transition to Ni 3$d_{xy}*$. Bands B and C are strong in E//z and are very weak in E $\perp$ z. (Hdmg)$_2{}^{2-}$ has some low-lying unoccupied orbitals. One of them has p_z symmetry, which split Ni 4p_z* into two orbitals. Thus, bands B and C correspond to the transitions to unoccupied orbitals of metal 4p_z* character with large mixing with ligand $\pi*$ orbital. For [(n-C$_4$H$_9$)$_4$N]$_2$-[Ni(II)(mnt)$_2$] (Figure 1b), the lowest band A is unambiguously assigned to a quadruple transition to Ni 3d$_{xy}*$ based on the polarization dependence; band A is strong in the spectra for (E//x, k//y) and (E//y, k//x) and very weak in the spectrum for (E//y, k//z) (not shown here), where k is the wave vector of incident photon. Band B is allowed for (E//z, k//x), and is assigned to out-of plane Ni 1s → 4p_z* transition. In contrast to Ni-(Hdmg)$_2$, no splitting of Ni 1s → 4p_z* transition is observed. This is because (mnt)$_2{}^{4-}$ has no low-lying unoccupied ligand orbital with p_z symmetry.
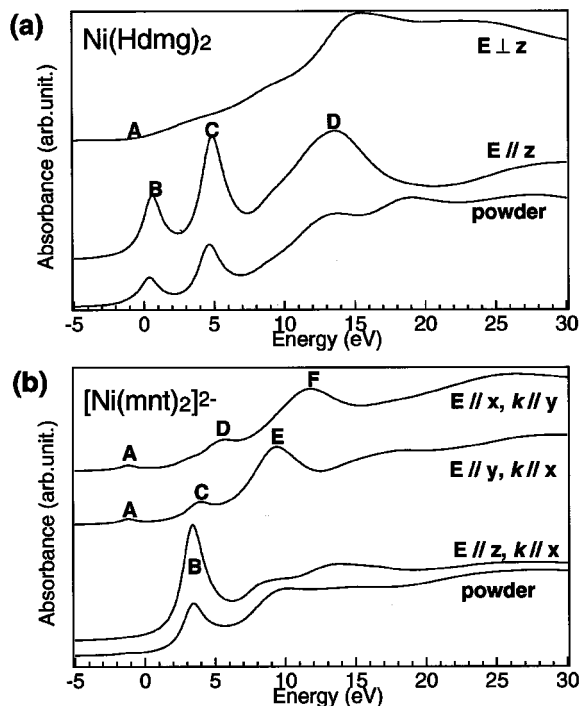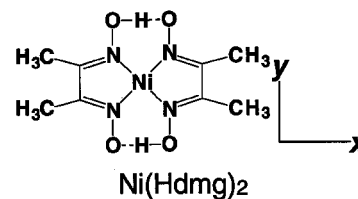
Figure 1. Polarized Ni 1s photoabsorption spectra of (a) Ni(Hdmg)$_2$ and (b) [(n-C$_4$H$_9$)$_4$N]$_2$[Ni(mnt)$_2$].

VI-B-4 Effect of Intermolecular Interaction on Resonant Behavior of Satellite Photoelectrons in Ni Planar Complexes

Yasutaka TAKATA, Takaki HATSUI *(Grad. Univ. Adv. Stud.)* **and Nobuhiro KOSUGI**

We have measured resonant photoelectron spectra of Ni(Hdmg)$_2$ [bis(dimethylglyoximato)nickel(II)] and Ni-(Hgly)$_2$ [bis(glyoximato)nickel(II)] in order to investigate the effect of the intermolecular interaction on resonant behavior of satellite photoelectrons. Both the complexes have nearly the same local bonding character around a Ni atom, but their Ni-Ni distances, 3.25 Å for Ni(Hdmg)$_2$ and 4.20 Å for Ni(Hgly)$_2$, are rather different. As expected, their Ni 2p photoabsorption spectra are very similar. Figure 1 shows the off-resonant (0), on-resonant photoelectron spectra (1-9) in the Ni 3p and 3s region and the normal Auger spectrum of Ni(Hdmg)$_2$. The enhanced satellite band (a-e) lowers the kinetic energy for the higher resonance energy and is converging to the normal Auger final state. This behavior is characteristic of the molecular solid system as observed in K$_2$Ni(CN)$_4$. In Ni(Hgly)$_2$ (not shown here), the photon energy dependence of the kinetic energy shift (slope) is relatively large, -0.42± 0.05, as in K$_2$Ni(CN)$_4$ (slope = -055). However, the slope is very small, -0.09±0.05 in Ni(Hdmg)$_2$ with strong intermolecular interaction as shown in Figure 1.

These results indicate that the slope is dependent on the intermolecular interaction.
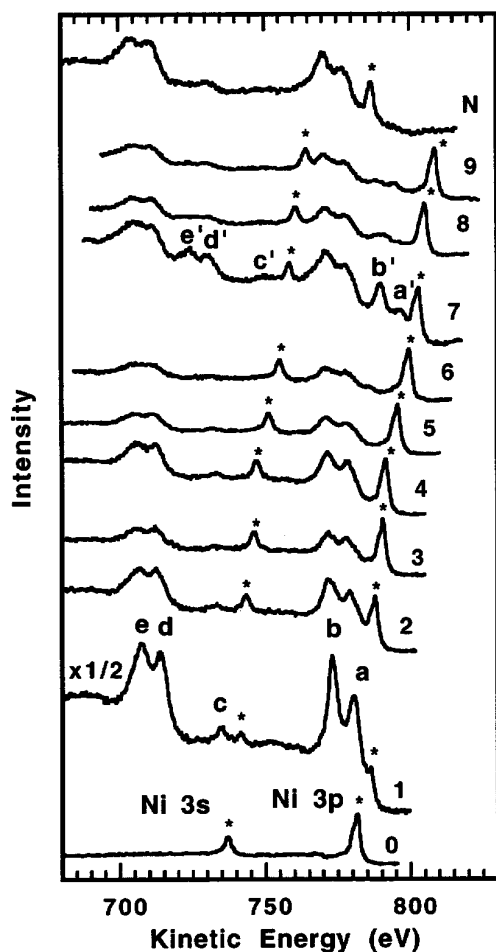
Figure 1. Off-resonant (0), on-resonant (1-9) photoelectron spectra in the Ni 3p and 3s region and the normal Auger spectra of Ni(Hdmg)$_2$.

VI-B-5 Resonant Photoelectron Spectra of Ni Metal Following the Ni 2p Excitation

Yasutaka TAKATA, Takaki HATSUI *(Grad. Univ. Adv. Stud.)* and Nobuhiro KOSUGI

We have measured resonant photoelectron spectra of Ni metal to get a unified interpretation of resonant behaviors of satellite photoelectrons at the Ni 2p edge. Figure 1 shows the off-resonant (0), on-resonant (1-6)

photoelectron spectra in the Ni 3p and 3s region and the normal Auger spectrum. The kinetic energies of all the enhanced satellite bands (a-e) shows linear dispersion as a function of the excitation energy, namely, constant binding energies, below the Ni $2p_{3/2}$ resonance maximum (0) and show constant kinetic energies above the maximum with the same energies as the $3p^{-1}3d^8$ ($L_3M_{2,3}M_{4,5}$) Auger final states. This is reasonable considering that the localized states are embedded in the continuum band. The "$2p^{-1}3d^{10}$" photoexcited state is not strongly localized, and both the "$3p^{-1}3d^9$" singly ionized satellite state and "$3p^{-1}3d^8$" doubly ionized Auger final state are well screened by the conduction electron. These behaviors are quite different from those of a strongly correlated system, NiO, and a molecular system such as K$_2$Ni(CN)$_4$ and Ni(Hdmg)$_2$.
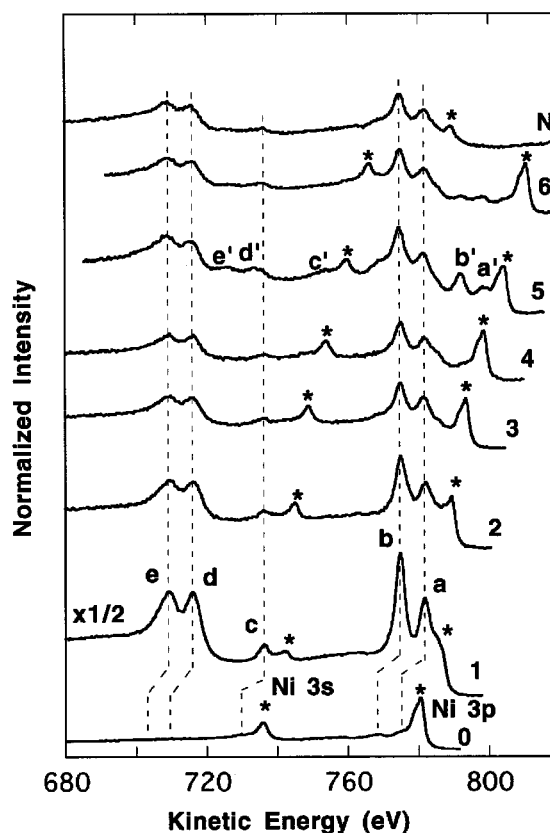
Figure 1. Off-resonant (0), on-resonant (1-6) photoelectron spectra in the Ni 3p and 3s region and the normal Auger spectra of Ni metal.

VI-C   Studies on Primary Photochemical/physical Processes Using Femtosecond Time-Resolved Electronic Spectroscopy

Ultrafast spectroscopy is playing an essential role in the elucidation of photochemical reactions. Thanks to recent advances of the laser technology, we are now even able to observe wavepacket evolution in the course of chemical reactions with femtosecond time-resolution. In this project, we are studying primary photochemical /physical processes in the condensed phase using several types of femtosecond time-resolved spectroscopy. We already constructed three experimental setups so far; a femtosecond time-resolved fluorescence up-conversion spectrometer, a femtosecond optical heterodyne detected impulsive stimulated Raman scattering (OHD-ISRS) spectrometer and a femtosecond UV-VIS-NIR transient absorption spectrometer. In this year, while continuing research with these setups, we have also constructed a setup for generating femtosecond mid-infrared pulses down

to 10 μm.

VI-C-1 Generation of a Femtosecond Pulse in the Near- to Mid-Infrared Region

Satoshi TAKEUCHI and Tahei TAHARA

We have constructed an experimental setup to generate a femtosecond pulse in the near- to mid-infrared region which is applicable to a variety of ultrafast vibrational spectroscopies (Figure 1). This system is driven by regeneratively-amplified Ti:sapphire laser pulses (800 nm, 100 fs, 0.5 mJ), and is composed of two parts: (i) optical parametric amplifier (OPA) to generate a near-infrared pulse and (ii) difference-frequency mixer to generate a mid-infrared pulse. In the first part, a seed pulse is generated by self-phase modulation in a thin sapphire plate. A near-infrared portion of the seed pulse (850-1000 nm region) is amplified in a double-pass β-BaB$_2$O$_4$ OPA pumped by the second harmonic at 400 nm. The group-velocity mismatch between the interacting pulses is minimized by employing the noncollinear interaction scheme. The energy of the seed pulse amounts to several microjoules after amplification. In the second part, the amplified seed pulse is mixed with the fundamental pulse (800 nm) in a AgGaS$_2$ crystal (0.5 mm thickness) to generate the mid-infrared pulse in the 4-11 μm region (900-2500 cm^{-1}). The wavelength of the mid-infrared pulse can be changed by simultaneous angle-tuning of the two crystals. The output spectra were measured by using a monochromator and a HgCdTe detector, and are shown in Figure 2. The bandwidth is about 80 cm^{-1} independent of the center wavelength, and it is determined mainly by the phase-matching condition of the AgGaS$_2$ crystal.
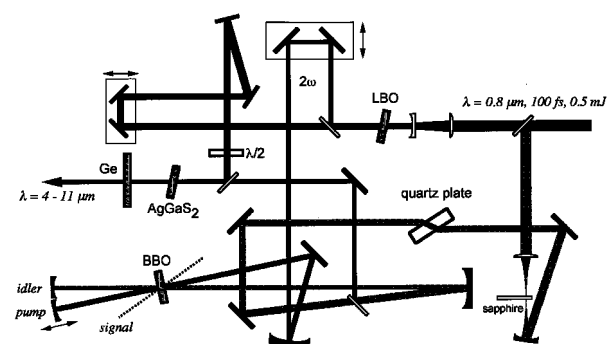
Figure 1. Apparatus for the femtosecond infrared pulse generation.
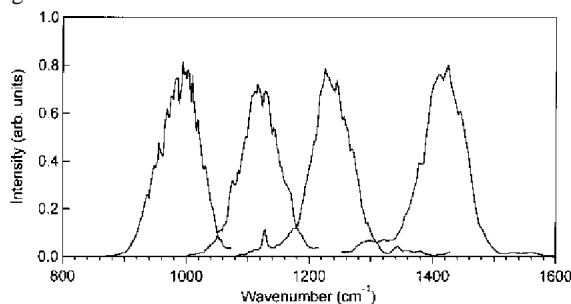
Figure 2. Spectra of the generated pulses in the mid infrared region.

VI-C-2 Femtosecond UV - VIS Fluorescence Study on the Excited-State Proton Transfer Reaction of 7-Azaindole Dimer

Satoshi TAKEUCHI and Tahei TAHARA

The dynamics of the excited-state proton transfer reaction of 7-azaindole dimer has been investigated in hexane with use of the femtosecond fluorescence up-conversion method. Time-resolved measurements were performed in a wide fluorescence wavelength region from near ultraviolet to visible (320-620 nm) (Figure 1). Three fluorescence components due to the dimer were observed in addition to the fluorescence from coexisting monomer. We assigned the first (τ = 0.2 ps) and the second (τ = 1.1 ps) fluorescence components to two different dimeric excited states having different transition moment directions. The decay of the second component agrees with the rise of the third component which is attributable to the fluorescence from the tautomeric excited state (τ = 3.2 ns) formed by the proton transfer reaction. The fluorescence spectra of these three excited states were reconstructed from time-resolved fluorescence traces taken at 27 wavelengths, and they show intensity maxima around 330, 350, and 490 nm, respectively. This sequential red-shift reflects the cascaded population relaxation after the photo-excitation. Combining the spectral data with fluorescence quantum yield data, the oscillator strengths of the three excited states were evaluated as 0.13, 0.048 and 0.023. We assigned the higher- and the lower-energy dimeric excited states to the "^1L_b" and "^1L_a" states of the dimer on the basis of the obtained photochemical information. The deuterium substitution effects were also examined for two isotopic analogues. It was concluded that the proton transfer proceeds exclusively from the lowest "^1L_a" excited state with a time constant of 1.1 ps, after the electronic relaxation takes place from the initially-populated "^1L_b" state to the "^1L_a" state (Figure 2). The excited-state reaction pathway as well as quantitative characterization of each excited state is discussed.
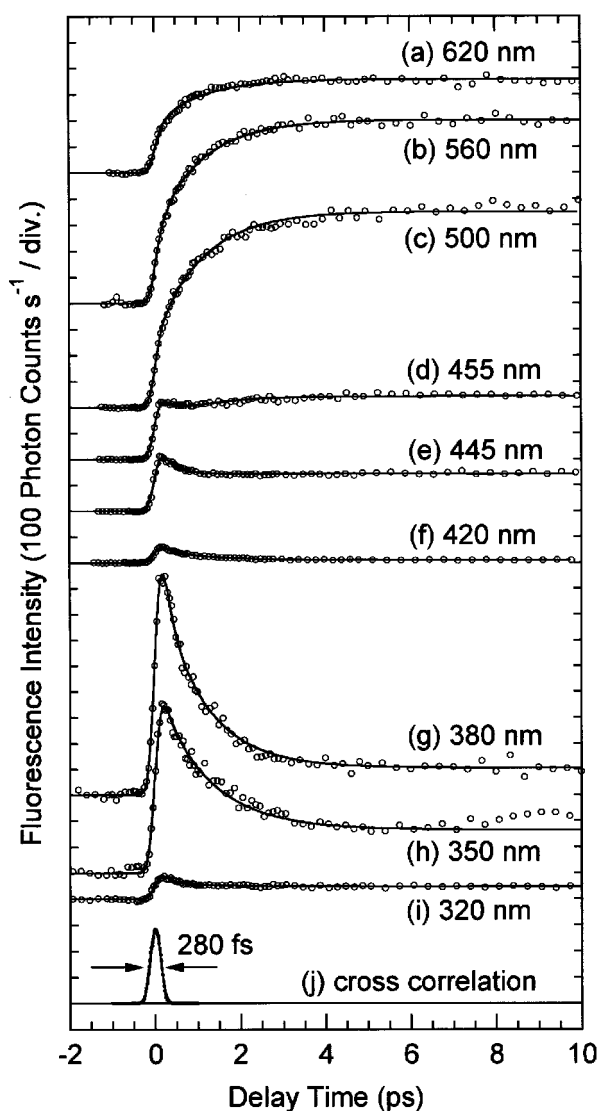
Figure 1. Femtosecond time-resolved fluorescence signals obtained from 7-azaindole in hexane (1×10^{-2} mol dm^{-3}, 270 nm excitation). Fluorescence signals at 620 nm (a), 560 nm (b), 500 nm (c), 455 nm (d), 445 nm (e), 420 nm (f), 380 nm (g), 350 nm (h), 320 nm (i), and a typical cross-correlation trace between the excitation and the gate pulses (j). The open circles are experimental data points, and the solid curves are results of the fitting analysis. The instrumental time resolution given by the fwhm of the cross-correlation trace is 280 fs.
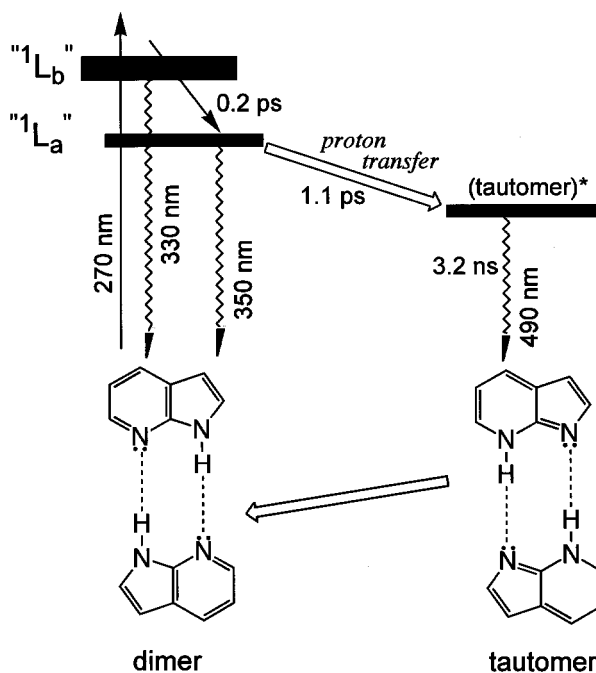
Figure 2. Schematic energy diagram illustrating the dynamics of the excited-state double proton transfer reaction of 7-azaindole dimer.

VI-C-3 Femtosecond Fluorescence Anisotropy Study of 7-Azaindole Dimer in Solution

Satoshi TAKEUCHI and Tahei TAHARA

Time-resolved anisotropy measurements have been widely utilized so far to investigate phenomena such as the orientational diffusion of molecules in solution and the migrational motion of excitations in solids. However, in the sub-picosecond time region, the orientational motion of molecules is negligible in solution. The anisotropy change observed in this short time region does not arise from the molecular motion but from the rotation of the excited-state transition moment direction itself, i.e., the change of the electronic excited state. Femtosecond time-resolved anisotropy measurements, therefore, can afford an unique experimental evidence which enables us to distinguish the internal conversion process from the dynamics within a single electronic excited state. In order to confirm the proton transfer reaction mechanism of 7-azaindole dimer which we propose, the fluorescence anisotropy of this molecule has been measured with a 280-fs time resolution (Figure 1). We observed a very rapid decrease of the anisotropy immediately after photoexcitation (0.2 ps), in addition to a slow component (12 ps) attributable to the orientational diffusion of the 7-azaindole dimer. Since the time constant of the rapid anisotropy change agrees with the observed lifetime of the "ultrafast" population decay component, we concluded that the internal conversion takes place from the initially-populated excited state to the lowest excited state having a different transition moment direction with a time constant of 0.2 ps. The quantitative analysis of the anisotropy data is now in progress to reveal relative directions of the two excited-state transition moments.
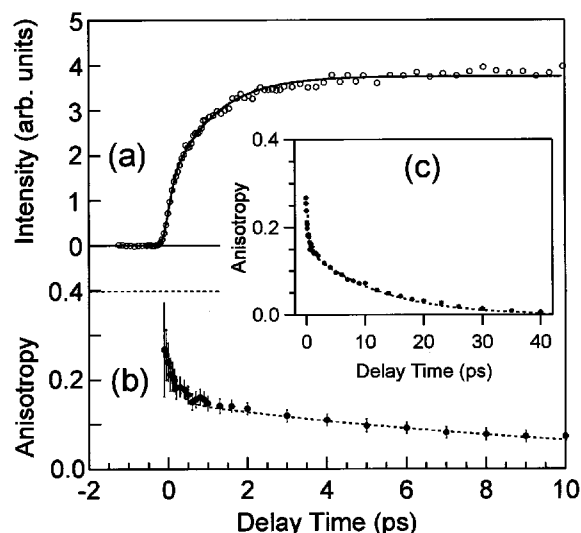
Figure 1. Time-resolved fluorescence signal (a) and fluorescence anisotropy (b) of 7-azaindole dimer in hexane at 500 nm. The longer-time behavior of the anisotropy is also shown in the inset (c). The dotted curve in the anisotropy data is the best-fitted biexponential function with decay time constants of 0.2 ps and 12 ps.

VI-C-4 Ultrafast Quenching of Biphenyl Fluorescence by Carbon Tetrachloride Observed with Time-Resolved Fluorescence Spectroscopy

Koichi IWATA *(Univ. Tokyo)*, **Satoshi TAKEUCHI and Tahei TAHARA**

Reaction kinetics of an ultrafast bimolecular reaction was successfully interpreted by the Smoluchowski model of diffusion-controlled reactions. When biphenyl is photoexcited to the first excited singlet (S_1) state in carbon tetrachloride solutions, it reacts with the solvent carbon tetrachloride. Because of this reaction, the fluorescence lifetime of biphenyl in carbon tetrachloride is anomalously shortened to a few picoseconds. We observed the kinetics of this ultrafast fluorescence quenching by using the fluorescence up-conversion method with the time resolution of 320 fs. Observed time dependence of the fluorescence signal from biphenyl in carbon tetrachloride is shown in the Figure 1 (dots). Although the observed decay curve was not fitted well with single exponential decay functions, it was well explained by a model function derived from the Smoluchowski model of diffusion-controlled reactions (solid curve). The fitting parameter for this analysis is distance R where the density of the reacting molecules becomes zero. The best fit was obtained when the distance R was 0.4 nm, which matched the actual size of the molecules well. The success of the Smoluchowski model suggests that the translational motion of biphenyl and carbon tetrachloride can be well described as a diffusion motion in a time scale of a few picoseconds.
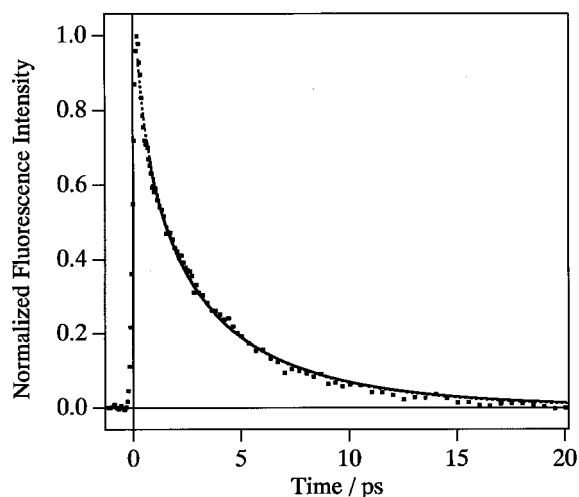
Figure 1. Observed fluorescence decay kinetics of biphenyl in carbon tetrachloride (dots). Decay kinetics simulated with the Simlukowski model of diffusion-controlled reaction is also shown (solid curve).

VI-C-5 Femtosecond Fluorescence from the Higher Excited State of Tetracene

Nilmoni SARKAR, Satoshi TAKEUCHI and Tahei TAHARA

In most of all cases, only fluorescence from the lowest excited singlet state is observed even if molecule is photoexcited initially to the higher excited singlet state. This rule, Kasha rule, was originally found for the steady-state fluorescence, but is also valid for time-resolved fluorescence up to picosecond time range. The implication of this rule is that the electronic relaxation from the higher excited state to the lowest one takes place much faster than fluorescence emission. However, if time-resolution of the measurement is high enough, it is expected that the fluorescence from the higher excited state is also observed before the electronic relaxation. With this idea, we studied fluorescence of tetracene with femtosecond time-resolution. Tetracene shows two prominent absorption bands in the ultraviolet-visible region. The absorption band in the ultraviolet is due to the ^1B_b-S_0 transition and the other in the visible is ascribed to the lowest ^1L_a-S_0 transition. We excited the molecule to the ^1B_b state with 270 nm excitation and found very short-lived fluorescence signal in the ultraviolet region where the intensity of steady-state fluorescence is negligible (Figure 1). The lifetime of this ultraviolet fluorescence was determined as 120 fs by fitting analysis which takes account of finite instrumental response. This lifetime agreed very well with rise of the ^1L_a (S_1) fluorescence observed in the visible region. We concluded that the fluorescence found in the ultraviolet is the fluorescence from the higher ^1B_b state and that the electronic relaxation from the ^1B_b state to ^1L_a state takes place with a time constant of 120 fs.
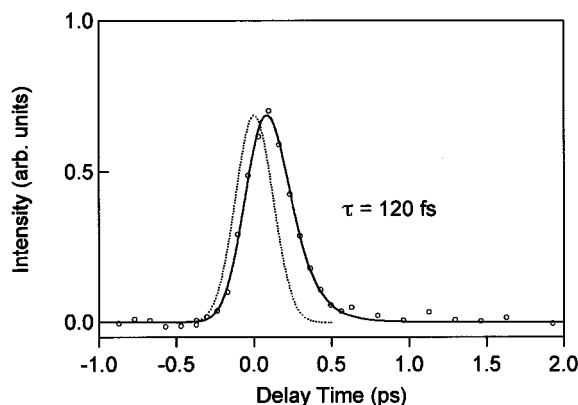
Figure 1. Femtosecond time-resolved fluorescence signal of tetracene at 340 nm (solid curve) and the instrumental response function (dotted curve).

VI-C-6 Ultrafast Relaxation Dynamics of Photo-excited Cu(II)(TMpy-P4) in Water

Sae Chae JEOUNG, Satoshi TAKEUCHI and Tahei TAHARA

We have conducted femtosecond pump-probe experiments to understand the relaxation process of a copper porphyrin, Cu(II)(TMpy-P4), in aqueous solution. It was found that both the spectral feature and the temporal behavior of the transient absorption strongly depend on the excitation density. From the comparison with a reference experiment for the solvent only, we concluded that the transient absorption signal obtained with the high excitation density arises not only from the excited-state dynamics of the porphyrin but also from solvated electrons generated from the water solvent. By carefully lowering the excitation density to remove the contribution from the solvated electrons, the transient absoption spectra purely due to Cu(II)(TMpy-P4) were obtained with photoexctation at the Soret band

(Figure 1). We observed a broad transient absorption band from 450 nm to near infrared region. This band exhibits a spectral sharpening in early delay times, and then becomes broader again. On the basis of the analysis of the spectral changes, the excited-state dynamics of Cu(II)(TMpy-P4) and a possible involvement of a five-coordinated complex with a water molecule are discussed.
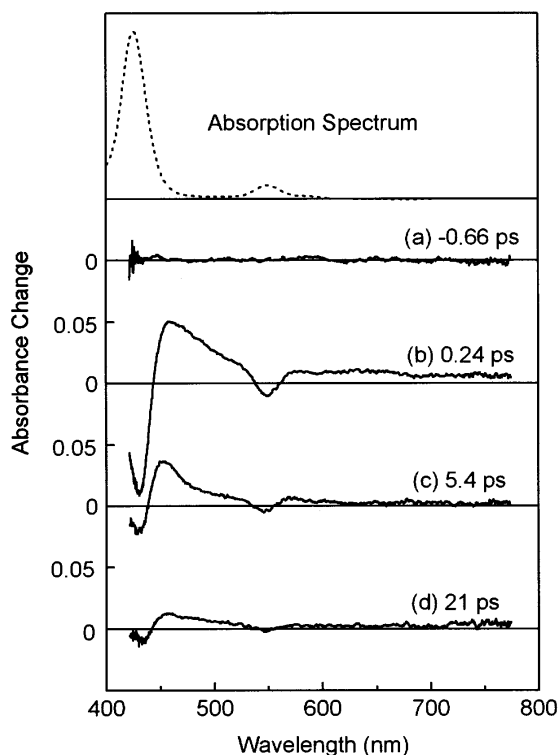
Figure 1. Transient absorption spectra of Cu(II)(TMpy-P4) in water measured at -0.66 (a), 0.24 (b), 5.4 (c), and 21 ps (d). Steady-state absorption spectrum of the porphyrin is also shown at the top.

VI-D Studies on Photochemical Reactions Using Picosecond Time-Resolved Vibrational Spectroscopy

Time-resolved vibrational spectroscopy is a very powerful tool for the study of chemical reactions. It often affords detailed information about the molecular structure of short-lived intermediates, which is not obtainable with time-resolved electronic spectroscopy. However, for molecules in the condensed phase, we need energy resolution as high as 10 cm^{-1} in order to obtain well-resolved vibrational spectra. This energy resolution is compatible only with time-resolution slower than picosecond because of the limitation of the uncertainty principle. In this sense, picosecond measurements are the best compromise between energy resolution and time resolution for time-resolved frequency-domain vibrational spectroscopy. In this project, we study photochemical processes and short-lived transient species by using picosecond time-resolved vibrational spectroscopy.

VI-D-1 Vibrational Dynamics in the Lowest Excited Triplet State Immediately after Intersystem Crossing

Atsuhiko SHIMOJIMA and Tahei TAHARA

Picosecond time-resolved spontaneous resonance Raman spectra of *all-trans* retinal were measured. Although it had been thought that the fluorescence background makes it difficult to obtain clear picosecond

Raman signals from retinal, we succeeded in observing transient Raman bands due to the T$_1$ state by using the probe laser which is rigorously resonant with the T-T absorption. In order to reveal the initial photodynamics of the T$_1$ state, quantitative analysis was carried out for the 1553 cm^{-1} and 1183 cm^{-1} bands of the *all-trans* T$_1$ state. The intensities of these two Raman bands increase with a time constant of 25 ps which is in good agreement with the reported intersystem crossing time constant of *all-trans* retinal. In addition, it was found

that their peak position and band width change with time (Figure 1). They show frequency up-shift and band narrowing in the time range from 5 ps to 30 ps. The peak shifts were well fitted to single exponential functions with time constants of 14 ps (1553 cm^{-1}) and 18 ps (1183 cm^{-1}). These observations imply that the T_1 state generated by the intersystem crossing is initially vibrationally hot, and then the vibrational cooling takes place within a few tens of picosecond in the triplet manifold.
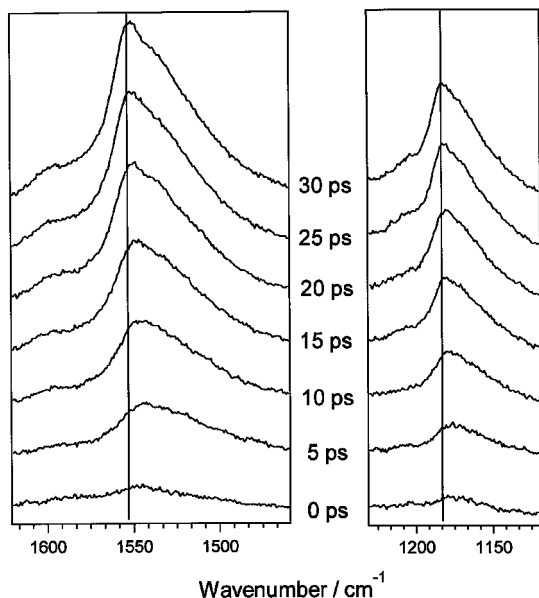
Figure 1. The initial photodynamics of the T_1 state of *all-trans* retinal observed in picosecond time-resolved Raman spectra (hexane solution, 10^{-3} mol dm^{-3}, pump 385 nm, probe 458 nm).

VI-D-2 Cis-Trans Photoisomerization Mechanism of Retinal Studied by Picosecond Time-Resolved Raman Spectroscopy

Atsuhiko SHIMOJIMA and Tahei TAHARA

Cis-trans photoisomerization of 9-cis and 13-cis retinal was studied by picosecond time-resolved resonance Raman spectroscopy. The time-resolved spectra were measured with the time and frequency resolution of 2 ps and 10 cm^{-1}, respectively, using an apparatus based on a picosecond mode-locked Ti: sapphire laser. The obtained spectra are shown in Figure 1. In the case of 9-cis retinal, the transient Raman bands assignable to the "all-trans" T_1 state slowly appear with a time constant of about 900 ps after photoexcitation, which indicates that cis-trans structural change takes place in the triplet manifold. On the other hand, with the photoexcitation of 13-cis retinal, the transient Raman signals attributable to the mixture of the "13-cis" and the "all-trans" T_1 states appear within several tens of picoseconds. In addition, the 1550 cm^{-1} band having contribution from both the "13-cis" and the "all-trans" T_1 states rises significantly faster than the 1182 cm^{-1} band which is solely due to the "all-trans" T_1 state. The time constant of rise of the 1182-cm^{-1} band agrees well with the intersystem crossing time of all-trans retinal. We concluded that the structural change from the 13-cis to the all-trans form takes place in the excited singlet state and that the "13-cis" and the "all-trans" T_1 states are separately generated from the S_1 state having each conformation. The cis-trans photoisomerization mechanism clarified in the present study is shown in Figure 2.
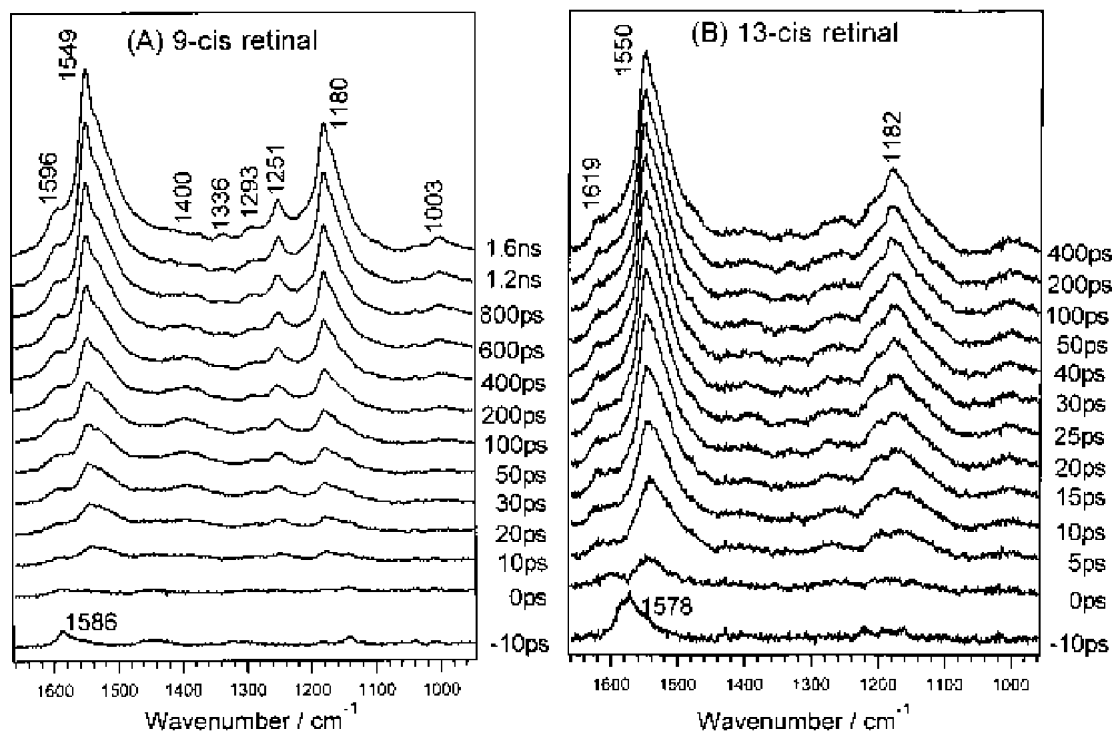
Figure 1. Time-resolved resonance Raman spectra of 9-cis (A) and 13-cis (B) retinal in hexane (10^{-3} mol dm^{-3}, pump 385 nm, probe 458 nm). Solvent Raman bands were subtracted from each spectrum.
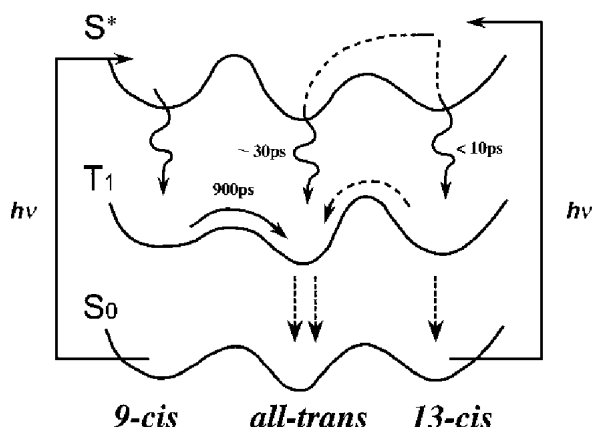
Figure 2. The cis-trans photoisomerization mechanism of retinal.

VI-D-3 Vibrational Cooling Dynamics of Solvated Structures of para-Nitroaniline in Acetonitrile

Kathaperumal MOHANALINGAM *(Waseda Univ.)*, Hiro-o HAMAGUCHI *(Univ. Tokyo)*, Atsuhiko SHIMOJIMA and Tahei TAHARA

Recently it has been shown that p-nitroaniline (pNA) in acetonitrile exists in two distinct solvated structures, the 1:1 form and 1:2 forms.[1] In the 1:1 form, acetonitrile is associated with the amino group of pNA while it is associated with both the amino and nitro groups in the 1:2 form. These two structures exhibit different charge transfer characteristics which are manifested in the difference in their absorption spectra. We have measured picosecond time-resolved Raman spectra of pNA in acetonitrile by using the pump laser at 400 nm and the probe laser at 454 nm. Under this experimental condition, only the 1:2 form is selectively photoexcited. Immediately after photoexcitation, we observed bleach and the following very fast recovery for the intensity of the Raman band due to the symmetric stretch of the nitro group in the ground-state 1:2 form (1315 cm^{-1}). In addition, the bandwidth of this band changed with the time delay, reflecting vibrational cooling taking place in the solvent structure. These observations are consistent with the result of the earlier femtosecond time-resolved absorption studies which indicated that very fast dissociation and reassociation processes occurs with a time constant as fast as 0.7 ps after photoexcitation of the 1:2 form.

Reference

1) K. Mohanalingam and H. Hamaguchi, *Chem. Lett.* 157 (1977); K. Mohanalingham and H. Hamaguchi, *Chem. Lett.* 537 (1997).

VI-E Development of Time-Resolved Spectroscopy Using Synchrotron Radiation

Synchrotron radiation affords photons in a wide energy region from X-ray to far-infrared, and is intrinsically produced in the form of a picosecond pulse train. The unique characteristics of synchrotron radiation are very attractive for time-resolved spectroscopy. In this project, by utilizing the combination of laser and synchrotron radiation, we attempt time-resolved measurements in energy regions which are not accessible only with the existing lasers. We have constructed a setup for subnanosecond time-resolved far-infrared measurements at beamline BL6B in UVSOR. In this year, we made attempts to measure time-resolved spectra of several solid samples with use of this set-up.

VI-E-1 Trial to Measure Time-Resolved Far-Infrared Spectra of '-(BEDT-TTF)$_2$ICl$_2$ Using Synchrotron Radiation

Tahei TAHARA and Akito UGAWA *(Univ. Florida, U.S.A.)*

Far-infrared spectra contain much information about low-frequency motion in the material including intermolecular vibrations in liquid and phonons in solid. It is highly desirable to develop time-resolved far-infrared spectroscopy, since it is expected to afford unique information on photo-induced processes in the material. In order to examine potentiality of synchrotron radiation for time-resolved far-infrared spectroscopy, we tried to measure time-resolved spectra of an organic semiconductor, '-(BEDT-TTF)$_2$ICl$_2$, by using a setup at beamline BL6B in our synchrotron radiation facility (UVSOR). In this measurement, we used picosecond laser pulses for the excitation of the sample, and utilized far-infrared synchrotron radiation for probing. The picosecond laser pulse was the second harmonic of the output of a mode-locked Nd:YAG laser which was synchronized to the synchrotron radiation. Far-infrared/infrared synchrotron radiation was introduced to a Michelson-type Fourier Transform spectrometer through a Si or a KRS-5 optical window. The pumping laser pulse and the probing synchrotron radiation pulse were focused and overlapped on the sample, and the reflected synchrotron radiation beam was detected with a bolomer. Time-resolution of the measurements was predominantly determined by the duration of synchrotron radiation which is about 1 ns. Figure 1 shows time-resolved difference reflectance spectra obtained from '-(BEDT-TTF)$_2$ICl$_2$ at 8K. With the irradiation of the laser pulse, the reflectance change was recognized for several phonon bands. The most prominent change was observed at the band around 230 cm^{-1}. This reflectance change, however, does not depend on the delay time, indicating that the relaxation time of the photo-induced change is much slower than the repetition rate of the photoexcitation (90 MHz). It is highly likely that the observed spectral change is due to the temperature change of the sample induced by the

laser irradiation.
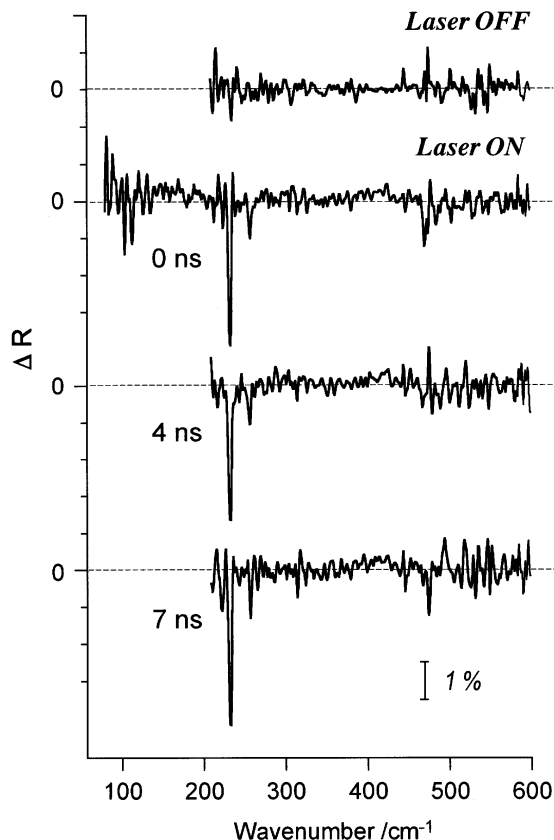
Figure 1. Time-resolved far-infrared spectra of '-(BEDT-TTF)$_2$ICl$_2$ at 8 K.

VI-F Synchrotron Radiation Stimulated Surface Reactions

Study of synchrotron radiation (SR) stimulated surface reaction is a promising topic in fundamental science, because dynamical processes induced by the photostimulated core-electron excitations on surfaces are scarcely explored so far. This field is important also in applied science, since the fundamental study is expected to develop the new techniques for semiconductor processing such as SR stimulated etching and SR stimulated epitaxial growth.

VI-F-1 The Direct Observation of Synchrotron Radiation Stimulated Desorption of Thin SiO$_2$ Films on Si (111) by Scanning Tunneling Microscopy

Takayuki MIYAMAE, Hironaga UCHIDA *(Toyohashi Univ. Tech.)*, **Tsuneo URISU and Ian H. MUNRO** *(UMIST and IMS)*

This is the first report of the use of scanning tunneling microscopy (STM) to study changes in the surface morphology during synchrotron radiation (SR) stimulated desorption of SiO$_2$ films on Si(111). An atomically flat and clear surface was obtained after two hours SR irradiation at a surface temperature of 700 °C as shown in Figure 1. The STM topograph indicates that the SR desorption mechanism is quite different for the thermal desorption of SiO$_2$. The non-formation of voids indicates that the desorption of oxygen atoms and molecules by SR excitation leaving volatile SiO is an important mechanism.
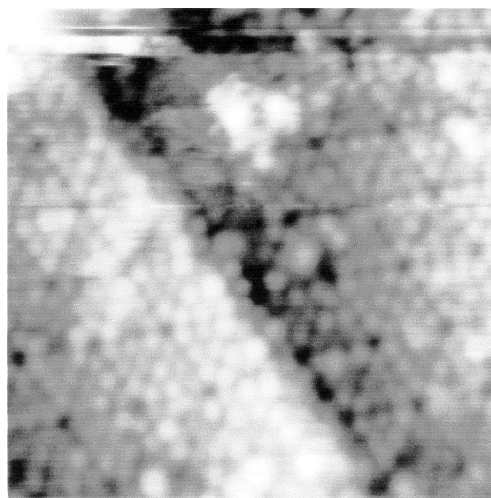
Figure 1. STM topograph of occupied states (sample vias = -2.1 V) of a Si (111) surface after 2 h SR-irradiation at 700 °C. Image size = 150 × 150 Å.

VI-F-2 Chemisorption of Deuterium on an Ultrathin Ge Film Deposited over Si(100)-2x1: Existence of a Dihydride Phase

Syed Irfan GHEYAS, Tsuneo URISU, Shinya HIRANO, Hidekazu WATANABE, Suehiro IWATA, Mutsumi AOYAGI, Mitsuhiro NISHIO *(Saga Univ.)* and Hiroshi OGAWA *(Saga Univ.)*

Adsorption of atomic deuterium on ultrathin Ge film deposited over Si(100) has been studied using Fourier transformed infrared reflection absorption spectroscopy and reflection high-energy electron diffraction (RHEED) measurements. Figure 1 shows the IR spectra of Ge/Si(100) as a function of deuterium exposure at 85 °C. At a low temperature of about 300 L, only one vibrational mode at about 1438 cm^{-1} can be observed clearly. This mode is assigned to GeD symmetric stretching. The RHEED pattern corresponding to an exposure of 320 L, which shows a strong 2 × 1 pattern, justifies this assignment. Notably, no Si-related peak was detected corresponding to this exposure. A deuterium exposure of 1200 L of higher, on the other hand, visibly weakens the GeD peak intensity. Interestingly, the IR spectra reveal a decrease in GeD intensity by about 40% but still no appearance of a Si-related peak as we proceed from Figures 1(a) to 1(c). We established that high atomic deuterium exposure on a Ge/Si(100) surface leads to a change in the RHEED pattern from 2 × 1 to 1 × 1. This change possibly is due to an overwhelming conversion on Ge monodeuterides to dideuteride. Etching of the Ge atoms has also clearly been observed.
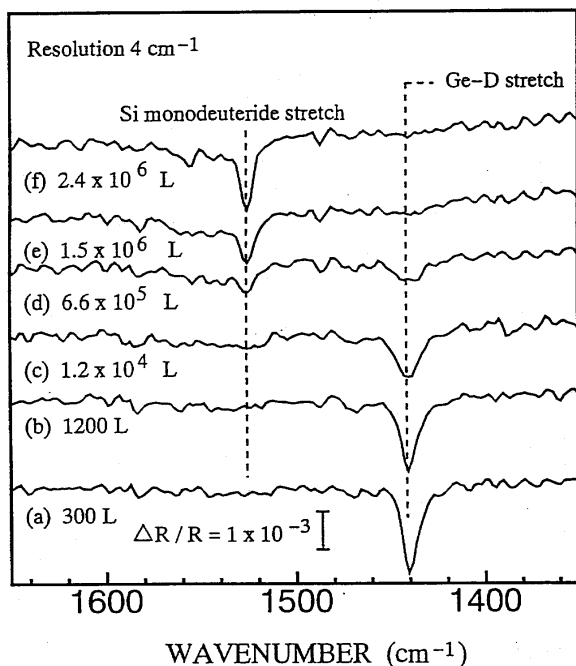
Figure 1. IR spectra taken after a series of deuterium exposures of Ge/Si(100) at 85 °C. All measurements were carried out at 85 °C.

VI-F-3 Structure of Hydrogen Terminated Si(100) Surfaces and Modification by Synchrotron Radiation Irradiation

Shinya HIRANO, Hideyuki NODA, Akitaka YOSHIGOE *(Japan Atomic Energy Research Institute)*, Syed Irfan GHEYAS *(Emory Univ.)* and Tsuneo URISU

The structure of the hydrogen (deuterium) saturation adsorbed Si(100)1×1 (H(D)-Si(100)1×1) surface generated at 400 K, and its change by annealing and synchrotron radiation (SR) irradiation were investigated by infrared reflection absorption spectroscopy (IRRAS) using CoSi$_2$ buried metal layer (BML) substrate and reflection high energy electron diffraction (RHEED) measurements. It was found that the structure of the H-Si(100)1×1 surface is disordered 3×1 consisting of coupled monohydride (H-Si-Si-H) + dihydride (H-Si-H) unit. By 650 K annealing, the D-Si(100)1×1 surface changes to 2×1 structure consisting of only D-Si-Si-D, which gives an SiD stretching vibration band with a sharp and symmetric shape peaked at around 1525 cm^{-1}. If the SR irradiation is added to the annealing of the D-Si(100)1×1 surface, the shape of the SiD stretching vibration band at 1525 cm^{-1} after 650 K annealing becomes broad and asymmetric. This is explained by that D-Si-D is etched (desorbed) by the SR irradiation.

VI-F-4 Design and Performance of a Multi-layered Mirror Monochromator in the Low Energy Region of Vacuum Ultra Violet

Harutaka MEKARU, Tsuneo URISU, Yoshiyuki TSUSAKA *(Himeji Inst. Tech.)*, Shin MASUI *(Sumitomo Heavy Industries Ltd.)*, Eijiro TOYOTA *(Sumitomo Heavy Industries Ltd.)* and Hisataka TAKENAKA *(NTT-AT)*

The vacuum ultra violet (VUV) photons in the SR can excite almost all the electronic states of molecules, so a large variety of chemical reaction channels different from that in the usual thermal-CVD are expected to be opened by the SR irradiation. In particular, core electrons, which cannot be excited using lasers are efficiently excited by the VUV photons in the SR. The excitation energy dependence of a photo-chemical reaction is important basic data. However it has not been sufficiently investigated in the VUV region, because of the difficulty of obtaining energy-tunable monochromatized light with sufficient photon flux in the VUV region.

In this work, a double-crystal-type MLM monochromator equipped with a C filter has been designed on the basis of trial fabrication of Mo/Si MLM and its performance has been evaluated by calculating what the basic characteristics such as output photon flux, resolution, monochromaticity and tuning range would be if the monochromator were set up as the part of the beamline (BL4A1) at the UVSOR. However,

considering a MLM monochromator to use in SR stimulated processes, it is known that extremely large total reflection components appear at less than 40 eV in the case of Mo/Si.

Therefore, a C thin-film filter was used to reduce drastically the low-energy background noise. The higher-order photons background noise is less than 4%. The calculated photon flux is $1 \sim 5 \times 10^{14}$ photons/s and the resolution is 5-9 eV. We conclude that the background noise due to the total reflection can be sufficiently reduced by using double MLM monochromator at low incident angles combined with the C thin-film filter.

VI-F-5 Construction of the Multilayered-Mirror Monochromator and the Beam Line for the Study of Synchrotron Radiation Stimulated Process

Harutaka MEKARU, Yoshiyuki TSUSAKA *(Himeji Inst. Tech.)*, **Takayuki MIYAMAE, Toyohiko KINOSHITA, Tsuneo URISU, Shin MASUI** *(Sumitomo Heavy Industries Ltd.)*, **Eijiro TOYOTA** *(Sumitomo Heavy Industries Ltd.)* **and Hisataka TAKENAKA** *(NTT-AT)*

[*Rev. Sci. Inst.* submitted]

The double crystal type multilayered-mirror (MLM) monochromator was developed and the beamline (BL4A1) using this monochromator was constructed at the UVSOR in the IMS. The low-energy background noise due to the total reflection component is reduced by using MLMs at low incident angles combined with a suitable thin-film filter. In the case of using Mo/Si MLMs and a C filter, the output beam photon flux, the monochromaticity, the low-energy background noise and the flux of the higher order photons were evaluated by measuring the transmission of the Al filter at around the Al $L_{2,3}$ absorption edge by a silicon photodiode and also by measuring the photo-emission spectra of Ta XPS spectra using the output beam as an excitation light source.

The transmission of the Al filter at around the Al $L_{2,3}$ absorption edge was measured by using the output beam of the monochromator as a function of the incident angle. The experimental results are compared with the calculation in Figure 1A. From the good agreement between the calculated and experimental results, it is concluded that the spectrum width should be almost equal to the calculated width (5 ~ 9 eV). The observed photo-emission spectra excited by output beam with the C filter at the incident angle of $\theta = 20°$ is shown in Figure 1B. The clear peak assigned to the Ta 5d state is observed indicating that the C filter reduces sufficiently the low-energy background.

It has been confirmed that the present MLM monochromator using Mo/Si MLM combined with C filter works well as predicted by the calculation. The output beam photon flux, the spectrum width, the low-energy background and the higher-order (second-order) photon background were evaluated to be 1.0×10^{12} (at 10 degree) ~ 1.5×10^{14} (at 55 degree) photons/s, 5 eV ~ 9 eV, less than 7.2% and less than 12%, respectively. We

conclude that the MLM monochromator beamline BL4A1 constructed here have sufficient performance for the study of the excitation-energy dependence in the SR stimulated process.
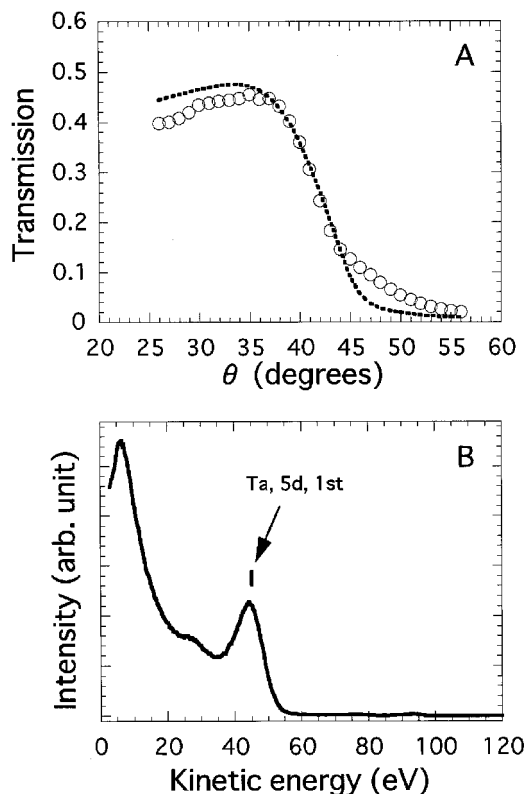
Figure 1. (A) The transmission of the Al filter in the vicinity of the Al $L_{2,3}$ absorption edge measured by using output beam of the monochromator for each mirror incident angle θ. ---: calculated value (the Al filter thickness of 180 nm and the transmission of the mesh holding the thin Al film of 74.8% are assumed) and $\bigcirc$: measured value, and (B) The photo-emission spectra of Ta measured by using the MLM monochromator output beam as the excitation light source. Mo/Si MLMs are used at θ = 20 degrees combined with the C filter (~120 nm thickness).

VI-F-6 Influence of Residual Fluorine Gases on the Adsorption of Atomic H on Si(100)-2×1 Surfaces

Hideyuki NODA, Shinya HIRANO, Youichi NONOGAKI, Mineo HIRAMATSU *(Meijo Univ.)* **and Tsuneo URISU**

We have investigated chemical reaction of atomic hydrogen (H) on Si(100)-2×1 surfaces and the effect of synchrotron radiation (SR) irradiation using buried metal layer - infrared reflection absorption spectroscopy (BML-IRRAS). In ultra high vacuum (UHV) chamber, we have found that a very small amount of residues influence Si clean surfaces. Figure 1 shows the intensity of each mass number measured by quadruple mass spectroscopy (QMS) in UHV chamber (2.0×10^{-10} Torr). The peak at the mass number of 19 for F component was observed, as shown in Figure 1. Figure 2 shows the IRRAS spectra of the time dependence after forming Si(100)-2×1 surface by gas source MBE

using disilane. As the time increased, the intensity of 820-1100 cm^{-1} peaks increased. These peaks are assinged to vibrations of Si-F (820 cm^{-1}), Si-F$_2$ and Si-F$_3$ (930 cm^{-1}), Si-F$_4$ (1010 cm^{-1}), respectively.[1] It is considered that residual fluorine gases or hydrogen fluoride adsorbes on Si clean surfaces.

The influence of residual fluorine or fluoride gases on the adsorption of atomic H on Si(100)-2×1 surfaces is under investigations.

Reference
1)C. J. Fang et al., *Phys. Rev. B* **22**, 6140 (1980).

Figure 2. Change of the IRRAS spectra of the Si(100) surface under fluorine or fluoride residual gases (a : after epitaxial growth, b : (a) + 30 min, c : (a) + 50 min).

Figure 1. Intensities of each mass number measured by QMS.

VI-G Ion Desorption Induced by Core-Electron Transitions Studied by Electron Ion Coincidence Spectroscopy Combined with Synchrotron Radiation

Ion desorption induced by core-electron transitions has been studied using energy-selected electron ion coincidence spectroscopy combined with synchrotron radiation. Auger electron photo-ion coincidence (AEPICO) and photoelectron photo-ion coincidence (PEPICO) spectroscopies proved to be an ideal tool for investigations of the ion desorption induced by core-level excitations. AEPICO results show that the character of the orbitals where holes are created, as well as the effective hole-hole Coulomb repulsion are important factors in the Auger-stimulated ion desorption from covalent molecules. The PEPICO spectroscopy, on the other hand, provided direct evidences of site-specific ion fragmentation induced by core-level excitations.

VI-G-1 Auger Electron Photoion Coincidence (AEPICO) Technique Combined with Synchrotron Radiation for the Study of Ion Desorption Mechanism in the Region of Resonant Transitions of Condensed H$_2$O

Kazuhiko MASE, Mitsuru NAGASONO, Shin-ichiro TANAKA, Tsuneo URISU, Eiji IKENAGA *(Hiroshima Univ.)*, **Tetsuji SEKITANI** *(Hiroshima Univ.)* **and Kenichiro TANAKA** *(Hiroshima Univ.)*

Auger electron photoion coincidence (AEPICO) technique has been applied for the study of H$^+$ desorption induced by resonant excitations of O 1s of condensed H$_2$O. The peak positions of the AEPICO yield spectrum at the $4a_1$ ← O 1s resonance ($h\nu = 533.4$ eV) are found to correspond to spectator-Auger transitions leaving (O 2s)$^{-2}$($4a_1$)^1, (O 2s)$^{-1}$(O 2p)$^{-1}$ ($4a_1$)^1, and (O 2p)$^{-2}$($4a_1$)^1 states. The H$^+$ AEPICO yield is greatly enhanced at $4a_1$ ← O 1s while suppressed at $3p$ ← O 1s ($h\nu = 537$ eV) as compared with that at the O 1s ionization ($h\nu = 560$ eV). On the basis of these results, the ultrafast ion desorption mechanism is

suggested to be favorable for the H$^+$ desorption at $4a_1$ O 1s, that is, the repulsive potential energy surface of the (O $1s)^{-1}(4a_1)^1$ state is responsible for the H$^+$ desorption. For H$^+$ desorption at $3p$ O 1s, spectator-Auger stimulated ion desorption mechanism is concluded to be probable. The suppression of the H$^+$ AEPICO yield is ascribed to the reduction of the hole-hole repulsion due to the shield effect of the $3p$ electron. These results demonstrate the power of AEPICO technique to clarify the mechanism of ion desorption induced by core-electron excitations.

VI-G-2 Study of Ion Desorption Induced by Resonant Core-Electron Excitation of Isolated NH$_3$ Monolayer Adsorbed on a Xe Film Using Auger Electron Photoion Coincidence Spectroscopy

Mitsuru NAGASONO, Kazuhiko MASE, Shin-ichiro TANAKA and Tsuneo URISU

Mechanism of ion desorption induced by resonant core-electron excitation of isolated NH$_3$ monolayer adsorbed on a Xe film (NH$_3$/Xe) is studied using Auger electron photoion coincidence (AEPICO) spectroscopy. The total ion yield spectrum of NH$_3$/Xe exhibits a threshold peak at the resonant excitation from N 1s to the $4a_1$ N-H antibonding orbital. The Auger electron spectrum of NH$_3$ at the $4a_1$ N 1s resonance is found to be mainly due to spectator Auger transitions. A series of AEPICO spectra at the $4a_1$ N 1s resonance is measured for the electron kinetic energies corresponding to the spectator Auger transitions. The AEPICO spectra show that the H$^+$ is the only desorbed ion species. The electron kinetic energy dependence of the H$^+$ AEPICO yield displays a structure similar to that of the spectator Auger electron spectrum. This result indicates that the H$^+$ desorption probabilities are independent of the spectator Auger final states. We suggest that the repulsive potential surface of the (N $1s)^{-1}(4a_1)^1$ state is responsible for the H$^+$ desorption, that is, ultrafast ion desorption mechanism is favorable in this system.

VI-H Photoionization Dynamics Studied by Electron Spectroscopy Combined with a Continuous Synchrotron Radiation Source

Molecular photoionization is a major phenomenon in vacuum UV excitation and provides a large amount of information on fundamental electron-core interactions in molecules. Especially, autoionizing and shape resonances become of main interest, since they often dominate photoabsorption cross sections and lead to various vibronic states which are inaccessible in direct ionization. In order to elucidate dynamical aspects of photoionization, we have developed a versatile machine for photoelectron spectroscopy. Introduction of a new methodology, two-dimensional photoelectron spectroscopy, allows us to investigate autoionization and predissociation of superexcited states of acetylene, nitric oxide, carbonyl sulfide, sulfur dioxide and so on. In this method, the photoelectron yield is measured as a function of both photon energy and electron kinetic energy (binding energy). The spectrum, usually represented as a contour plot, contains rich information on photoionization dynamics.

VI-H-1 Spectator- and Participant-Like Behavior of a Rydberg Electron on Predissociation of Superexcited States of OCS

Yasumasa HIKOSAKA, Hideo HATTORI and Koichiro MITSUKE

[*J. Chem. Phys.* submitted]

Predissociation of superexcited states of OCS is studied by two-dimensional photoelectron spectroscopy using synchrotron radiation in the photon energy range of 15-16.5 eV. A two-dimensional photoelectron spectrum exhibits two kinds of characteristic patterns both of which are ascribed to autoionization of sulfur atoms. To clarify the point, we show a photoelectron spectrum of Figure 1 which is obtained as a cut through the two-dimensional spectrum along the electron kinetic energy axis at the phootn energy of 15.95 eV. The superexcited atom S* is produced by predissociation of a Rydberg state OCS*(R_B) converging to OCS$^+(\widetilde{B}^2\ ^+)$. The pattern of the first kind results from predissociation processes in which the effective principal quantum number n of the Rydberg electron is almost conserved.

This suggests that the Rydberg electron behaves as a spectator because of its negligibly weak interaction with the ion core (spectator predissociation). On the contrary, n of S* does not accord with that of OCS*(R_B) in the pattern of the second kind, indicating that the Rydberg electron participates directly into the electron exchange mechanism controlling conversion from OCS*(R_B) to a predissociating state (participant predissociation). With increasing n, OCS*(R_B) decays more preferentially by the spectator than by the participant predissociation. The spectator predissociation of OCS*(R_B) proceeds through a two-step conversion which involves Rydberg states converging to OCS$^+(\widetilde{A}^2\ $ and $\widetilde{X}^2\ )$ and a dissociative multiple-electron-excited state OCS*(SAT) asymptotically correlating with S* + CO($\widetilde{X}^1\ ^+$). In contrast, the participant predissociation may be accounted for by a direct conversion from OCS*(R_B) to OCS*(SAT). The quantum yields are estimated from Figure 1 to be 0.07 and 0.02 for the participant and spectator predissociation, respectively, at the incident photon energy of 15.95 eV where OCS*(R_B) states with $n \sim 12$ lie. A simulation is performed to reproduce the partial cross section curve for the spectator predissociation by using a model in which the decay

rates for the participant and spectator predissociation are assumed to be proportional to n^{-3} and n^0, respectively. The simulated and experimental cross section curves are in good agreement with each other at the photon energy higher than 15.8 eV.
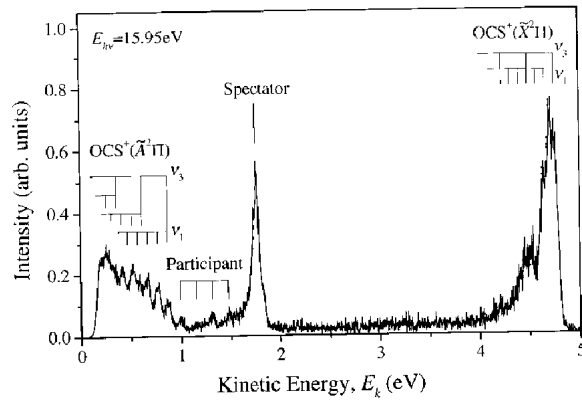
Figure 1. Photoelectron spectrum of OCS at the photon energy of 15.95 eV where OCS*(R_B) states with $n \sim 12$ are located.

VI-I Laser Photionization of Polarized Atoms Produced by Excitation with Synchrotron Radiation

In conventional photoionization experiments, the most standard method has generally been taken to be measurement of energy and angular distributions of photoelectrons from randomly oriented (unpolarized) atoms or molecules. However, information obtained from these experiments is insufficient, since the initial state constituted of atoms and photons is not selected and the internal properties of final photoions and electrons are not analyzed. In this project, we have performed photoelectron spectroscopy of polarized atoms using linearly-polarized laser light, aiming at complete quantum-mechanical photoionization experiments. Initial excitation with a linearly polarized synchrotron radiation permits ensemble of atoms to be aligned along the electric vector of the light. From an angular distribution of photoelectrons from polarized atoms, we are able to gain insight into the magnitude and phase shift difference of dipole transition moments of all final channels which are allowed by selection rules.

VI-I-1 Laser Photoionization of Polarized Ar Atoms Produced by Excitation with Synchrotron Radiation

Koichiro MITSUKE, Yasumasa HIKOSAKA *(Inst. for Mater. Struct. Sci.)* **and Kota IWASAKI**

Photoionization dynamics of poalrized Ar atom has been studied by photoelectron spectroscopy. Linearly polarized synchrotron radiation is used to pump a ground state atom to Rydberg states lying below the first ionization potential of Ar (15.759 eV). The polarized Ar atom is then ionized by absorbing a single photon of a Nd:YAG laser (= 532 nm) which is also linearly polarized. This photoionization process can be expressed by

$$\text{Ar} \xrightarrow{\text{Synchrotron Radiation}} \text{Ar*}(_0, J_0 = 1) \xrightarrow{\text{Laser}} \text{Ar*}_{f}, J_f = \tfrac{1}{2} \text{ or } \tfrac{3}{2} + e^-(\ell, j) \quad (1)$$
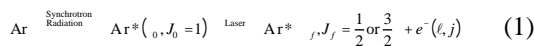
where J_0 and J_f are the total angular momentum quantum numbers of Ar* and Ar+, respectively, $_0$ and $_f$ are the sets of quantum numbers other than J_0 and J_f, respectively, ℓ is the orbital angular momentum quantum number of the photoelectron e^-, and j is the total angular momentum quantum number of e^-. The total angular momentum quantum number J of the final state, which is given by a relation of $J = J_f + j$, is restricted to 0, 1, and 2 from selection rules of the electric dipole transition. We have measured a two-dimensional spectrum as shown in Figure 1. Major spots are found to form two straight lines with a slope

of unity which are attirbuted to two final ionic states of Ar+ ($^2P_{1/2}$, $^2P_{3/2}$). Rotating the direction of the electric vector of the laser allows us to measure the angular distribution of energy-analyzed photoelectrons from a particular Ar* state. It is possible in some cases that we can estimate the dipole transition moments involving partial waves of photoelectrons designated by a combination of three angular momenta ℓ, j and J.
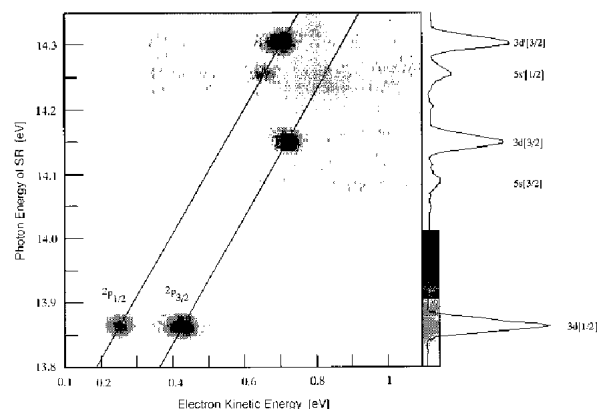
Figure 1. Laser-ionization two-dimensional photoelectron spectrum of polarized Ar atoms prepared by excitation with synchrotron radiation.

VI-I-2 Laser Photoionization Electron Spectroscopy of Polarized Kr Atoms Excited with Synchrotron Radiation

Kota IWASAKI, Yasumasa HIKOSAKA *(Inst. Mater. Struct. Sci.)* **and Koichiro MITSUKE**

Laser photoionization spectroscopy of polarized Kr atoms have been carried out to study spin-orbit interactions of a many-electron system. Krypton atoms are excited to Rydberg states with synchrotron radiation (= 900-950 nm) and aligned along the electric vector of the light. The beam of a Nd:YAG laser (= 532 nm) intersects the synchrotron radiation beam at 90° in a gas cell and ionizes the polarized Kr atoms. Photoelectrons emitted in the perpendicular direction to both the synchrotron radiation and laser beams are detected by using 160° spherical electrostatic energy analyzer.

We have measured a two-dimensional spectrum as shown in Figure 1. Major spots are found to form two straight lines with a slope of unity which are attirbuted to two final ionic states of $Kr^+(^2P_{1/2}, {}^2P_{3/2})$. Since every Rydberg state is properly described by a J_c- coupling scheme, its ion core is assumed to release an excited electron without changing J_c on laser ionization. Here, the total angular momentum quantum number J_c of the ion core takes a value of either 1/2 or 3/2. We can therefore expect the conservation of the total angular momentum between J_f of the final Kr^+ state and J_c of the Rydberg state. However, several spectral features in Figure 1 appear to show a reverse trend. For example, the intensity of $Kr^+(^2P_{1/2})$ from the $5d[1/2]$ Rydberg state is higher than that of $Kr^+(^2P_{3/2})$, though Jc of this Rydberg state is 3/2. There are two possible interpretations for this observation: mixing of $J_c = 1/2$ and 3/2 components in the initial Rydberg state, or angular momentum exchange between the ejected electron and the ion core during photoionization.
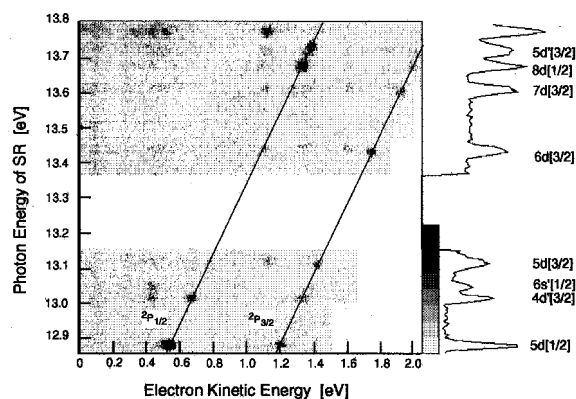
Figure 1. Laser-ionization two-dimensional photoelectron spectrum of polarized Kr atoms prepared by excitation with synchrotron radiation.

VI-J Vacuum UV Spectroscopy Making Use of a Combination of Synchrotron Radiation and a Mode-Locked or Pulsed UV Laser

An ultraviolet laser system has been developed which synchronizes precisely with the undulator radiation from the storage ring of the UVSOR facility. A mode-locked Ti:sapphire laser is made to oscillate at the frequency of the ring in a multibunch operation mode. The delay timing between undulator and laser pulses can be changed from 0 to 11 ns. The following two synchrotron radiation-laser combination studies have been performed. (1) Two-photon ionization of helium atoms studied as the prototype of the time-resolved experiment, and (2) fluorescence excitation spectroscopy of $N_2^+(X\ ^2\ _g^+)$ ions produced by synchrotron radiation photoionization of N_2 or N_2O. On the other hand, we have developed another system, a pulsed dye laser pumped by an excimer laser, for synchrotron radiation-laser combination experiments. The second harmonic of the dye laser is tunable at 265-280 nm with a pulse energy of ca. 2 mJ pulse^{-1} at a repetition rate of 10-100 Hz. This laser system is mainly devoted to observing neutral species produced by neutral or ionic photofragmentation induced by synchrotron radiation excitation of molecules. This year, $S(3s^23p^4\ ^3P_{J''}, J'' = 0, 2)$ from Rydberg states of OCS is detected by resonance enhanced multiphoton ionization (REMPI) spectroscopy.

VI-J-1 Pump-Probe Spectroscopy of N₂ and N₂O by Using a Laser-Synchrotron Radiation Combination Technique

Koichiro MITSUKE, Masakazu MIZUTANI, Hiromichi NIIKURA *(Grad. Univ. Adv. Stud.)* **and Kota IWASAKI**

Gas-phase N_2 or N_2O is photoionized with the fundamental light of an undulator radiation into $N_2^+(X\ ^2\ _g^+,\ '' = 0)$ which is then probed by laser induced fluorescence excitation spectroscopy in the laser wavelength region of the $(B\ ^2\ _u^+,\ ' = 0) \leftarrow (X\ ^2\ _g^+,\ ''$ = 0) transition at 389-392 nm. The fluorescence excitation spectra of N_2^+ exhibit two maxima due to the *P* and *R* branches in which rotational lines are heavily overlapped. By fixing the laser wavelength at the maximum position of the *P* branch, partial cross sections for production of $N_2^+(X\ ^2\ _g^+,\ '' = 0)$ are measured as a function of the undulator photon energy. The cross section curve for N_2^+ from N_2 shows peaks originating from transitions to autoionizing Rydberg states converging to $N_2^+(A\ ^2\ _u,\ = 0$ or 1). In the case of N_2O, several Rydberg states converging to $N_2O^+(C\ ^2\ ^+,\ _1 = _2 = _3 = 0)$ are discernible in the cross section curve for N_2^+, as shown in Figure 1. It is likely that these Rydberg states autoionize into $N_2O^+(B\ ^2\ )$ which is subsequently predissociated by a repulsive

state correlating with $N_2^+(X\,^2\Sigma_g^+,\ v''=0)$ + O.
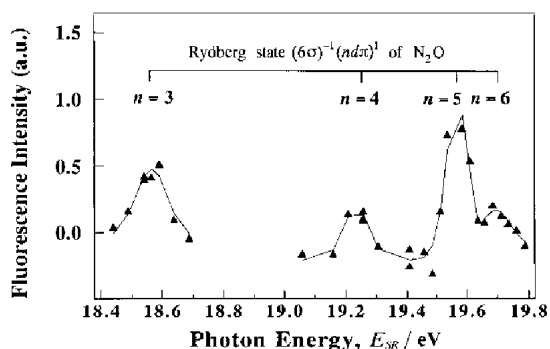
Figure 1. Photodissociation cross section curve of $N_2^+(X\,^2\Sigma_g^+,\ v''=0)$ obtained by plotting the laser induced fluorescence count rate of N_2^+ produced from N_2O as a function of the undulator photon energy.

VI-J-2 Apparatus for Resonance Enhanced Multiphoton Ionization Spectroscopy of Neutral Fragments Produced by VUV Photoexcitation

Masakazu MIZUTANI, Hiromichi NIIKURA *(Grad. Univ. Adv. Stud.)*, **Kota IWASAKI and Koichiro MITSUKE**

We have developed pump-probe spectroscopy making use of the combination of UV laser and synchrotron radiation to investigate neutral dissociation of molecular superexcited states. Superexcited molecules are produced by excitation with monochromatized synchrotron radiation and neutral fragments resulting from predissociation are observed by means of (2+1)-resonance enhanced multiphoton ionization (REMPI) spectroscopy.

Undulator radiation emitted from beamline BL3A2 of UVSOR is crossed perpendicularly with a molecular beam discharged from a pulsed nozzle. Produced ions are extracted toward electrode 1 by a retarding field between electrodes 1 and 2. A part of neutral fragments produced by VUV excitation are sampled through an aperture of electrode 2 and ionized by a frequency-doubled dye laser (1-2 mJ pulse^{-1}) focused with an f = 500 mm lens on the space between electrodes 2 and 3. Ions produced by (2+1)-REMPI of the neutral fragments are detected with a quadrupole mass filter equipped with a channeltron electron multiplier.

The most serious problem in this REMPI experiment is that the real signal is smeared out by the background ion counts which originate from undulator radiation alone. In the case of detection of $S(3s^23p^4\,^3P_2)$ from superexcited OCS molecules, the background count rate of S^+ is not less than 0.07 cps. These ions may be produced by electron impact ionization of residual gas of OCS near the aperture of electrode 2, since a number of electrons produced by VUV photoionization are accelerated to electrode 2. In order to suppress the background, we are planning to replace the ion lens system.
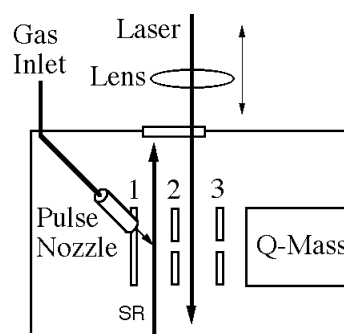
Figure 1. Schematic experimental setup for REMPI spectroscopy of neutral fragments produced by synchrotron radiation excitation.

VI-J-3 Laser Spectroscopy of Neutral Fragments from Superexcited States Prepared by Synchrotron-Radiation Photoexcitation

Hiromichi NIIKURA *(Grad. Univ. Adv. Stud.)*, **Masakazu MIZUTANI, Kota IWASAKI and Koichiro MITSUKE**

We have measured a REMPI spectrum of $S(3s^23p^4\,^3P_{J''},\ J''=0,2)$ dissociated from superexcited states of OCS prepared by photoexcitation with undulator radiation (BL3A2, UVSOR) in the range of 13-17 eV. The spectral resolution of the second harmonic of a probe laser was 0.015 nm. Figure 1 shows a REMPI spectrum of $S(3s^23p^4\,^3P_2)$ as a function of the probe laser wavelength in the region involving the two-photon transitions, $S(3s^23p^35p\,^3P_{J'}) \leftarrow S(3s^23p^4\,^3P_2)$. The undulator photon energy was fixed at 16.5 eV. The maximum at 269.290 nm is considered to comprise two peaks resulting from transitions from $S(3s^23p^4\,^3P_2)$ to $S(3s^23p^35p\,^3P_1)$ and to $S(3s^23p^35p\,^3P_2)$, though they are not separated because of a low signal-to-background ratio. As well as $S(3s^23p^4\,^3P_2)$, we have been able to detect the REMPI signal of $S(3s^23p^4\,^3P_0)$ at 271.375 nm where the two-photon transition from $S(3s^23p^4\,^3P_0)$ to $S(3s^23p^35p\,^3P_0)$ is allowed. Next, we fixed the laser wavelength at the maximum of Figure 1, *i.e.*, 269.290 nm, and measured the REMPI signal intensity as a function of the energy of the undulator radiation in the range of 13-17 eV. The resultant spectrum is considered to represent a relative photodissociation cross section curve for the formation of $S(3s^23p^4\,^3P_2)$ from OCS. Band features existing at 13-16 and 16-17 eV are ascribed to the Rydberg series converging to the $B\,^2\Sigma^+$ and $C\,^2\Sigma^+$ states, respectively, of OCS$^+$. In summary, we can obtain direct evidence for the first time for the formation of nonfluorescing and non-autoionizing neutral species dissociated from molecular superexcited states, by means of pump-probe spectroscopy combining synchrotron radiation and laser.
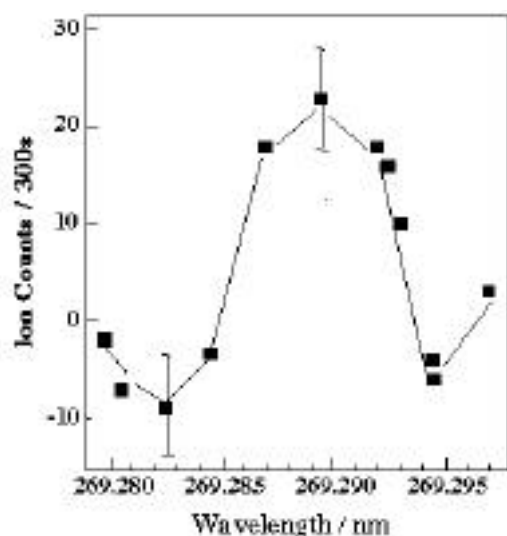
Figure 1. Laser REMPI spectrum of $S(3s^2 3p^4\ ^3P_2)$ produced by photoexcitation at the undulator photon energy of 16.5 eV.

VI-K Monochromator Newly Developed on Beamline BL2B2 in UVSOR

A grazing incidence monochromator has been constructed which supplies photons in the energy region from 20 to 200eV. This monochromator will bridge the energy gap between beamlines BL3A2 and BL8B1, thus providing for an accelerating demand for the high-resolution and high-flux photon beam from the research field of photoexcitation of inner-valence electrons or *L*-shell electrons in the third-row atom. A resolving power (*E/ E*) of 5000 and photon flux of more than 10^{10} photons s^{-1} are expected at a 100 mA ring current.

VI-K-1 Design of an 18 m Spherical Grating Monochromator at UVSOR

Hideo HATTORI, Hiroaki YOSHIDA *(Hiroshima Univ.)* **and Koichiro MITSUKE**

An 18m spherical grating monochromator (SGM) has been constructed on the bending-magnet beamline BL2B2 of the UVSOR facility. Figure 1 shows the outline of the monochromator which consists of chambers for a prefocusing mirror (M1), an entrance slit (S1), gratings, an exit slit (S2), and a refocusing mirror (M4). Three gratings (G1-G3) and two mirrors (M2, M3) are accommodated in the grating chamber. The energy range of 20 - 200 eV is covered by exchanging G1-G3. When G3 is chosen, M2 and M3 are made to act as optical filters to reduce the second and higher-order lights. A computer controls mechanical motion for the wavelength scanning, *i.e.* rotation of the gratings and translation of the exit slit. From a preliminary optical adjustment, the zero-order light is found to be focused into a 1×1 mm^2 square spot at the focusing point. We are planning to connect a differential pump (XIA, DP-03.1) with the refocusing mirror chamber. In spite of a relatively short pump length we may attain a pressure difference of six orders of magnitude between this chamber and an experimental station, since this pump has the line of sight passing through the active pumping region of a Penning style ion pump.
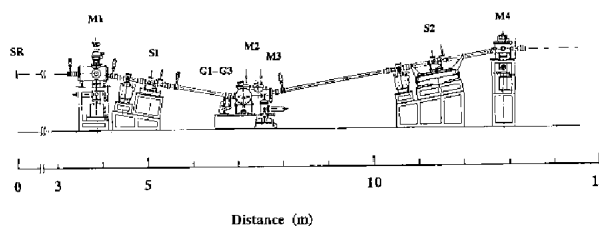
Figure 1. Schematic side view of the 18 m spherical grating monochromator at beamline BL2B2. SR, synchrotron radiation source; M$_1$, spherical mirror; S1, entrance slit; G1-G3, spherical gratings; M2 and M3, plane mirrors; S2, exit slit; M4, toroidal mirror.

VI-L Ultraviolet Photoelectron Spectroscopy on Organic Thin Films Using Synchrotron Radiation

The electronic structure and molecular orientation of organic thin films were investigated by angle-resolved UPS with synchrotron radiation. Furthermore corresponding spectroscopies, such as low-energy electron transmission, electron energy loss spectroscopy and Penning ionization electronspectroscopy, were used in investigating the electronic states of the thin films. The radiation inducedreaction at the surface of organic films were also studied by UPS and ion time-of-flight spectroscopy.

VI-L-1 Angle-Resolved UV Photoelectron Spectra (UPS) of Thin Films of Perylene-3,4,9, 10-Tetracarboxylic Dianhydride on MoS₂

Yasushi AZUMA *(Chiba Univ.)*, **Takehiko HASEBE** *(Chiba Univ.)*, **Takayuki MIYAMAE, Koji K. OKUDAIRA** *(Chiba Univ.)*, **Yoshiya HARADA** *(Chiba Univ.)*, **Kazuhiko SEKI** *(Nagoya Univ.)*, **Eizi MORIKAWA** *(Louisiana State Univ.)*, **Volker SAILE** *(Louisiana State Univ.)* **and Nobuo UENO**

Angle resolved UV photoelectron spectra (ARUPS) were measured for thin films of perylene-3,4,9,10-tetra-carboxylic dianhydride (PTCDA) deposited on cleaved MoS₂ Surfaces. The take-off angle ( ) dependence of the photoelectron intensity of the highest band showed a sharp maximum at = 32-34°. A spectral feature of the binding energy at ~ 8.9 eV, which is believed to originate from a State, showed a remarkably different dependence from that of the band. A quantitative analysis of the observed dependencies clearly indicates that (a) the feature at ~ 8.9 eV originates from the oxygen 2p nonbondipg states and (b) the molecules lie flat on the substrate surface.

VI-L-2 Temperature Dependence of Photo-electron Angular Distribution from Thin Films of Chloroaluminum Phthalocyanine on MoS₂

Yasushi AZUMA *(Chiba Univ.)*, **Masahiko TSUTSUI** *(Chiba Univ.)*, **Satoshi KERA** *(Chiba Univ.)*, **Masaru AOKI** *(Univ. Tokyo)*, **Takayuki MIYAMAE, Koji K. OKUDAIRA** *(Chiba Univ.)*, **Yoshiya HARADA** *(Chiba Univ.)* **and Nobuo UENO**

Angle-resolved UV photoelectron spectra were measured for thin films of chloroaluminum phthalo-cyanine deposited on cleaved MoS₂ Surfaces. The take-off angle ( ) dependence of the photoelectron intensity of the highest band showed a remarkable sharpening upon cooling the film, indicating that thermal excitation of molecular vibrations gives a considerable broadening of the photoelectron angular distribution. The dependence observed at ~ 120 K agrees well with that calculated.

VI-L-3 Photoemission Study of Pristine and Photodegraded Poly(Methyl Methacrylate)

Koji K. OKUDAIRA *(Chiba Univ.)*, **Shinji HASEGAWA, Phillip T. SPRUNGER** *(Louisiana State Univ.)*, **Eizi MORIKAWA** *(Louisiana State Univ.)*, **and Volker SAILE** *(Louisiana State Univ.)*

Degradation of poly(methyl methacrylate) (PMMA) thin films by vacuum ultraviolet (VUV) monochromatic synchrotron radiation was investigated by ultraviolet photoelectron spectroscopy. The photodegradation reaction was analyzed, for the first time, by different spectrometry techniques and ab initio molecular orbital calculations. It is concluded that the main degradation mechanism in PMMA by VUV photons is ascribed to the disappearance of ester groups and formation of double bonds in the polymer chain. The hal product of the degradation seems to possess a relatively dch conjugation of unsaturated bonds. The rate constant of the degradation by VUV photons is evaluated to be 2.4×10^{-17} photons^{-1} cm^2.

VI-L-4 Site-Specific Chemical-Bond Scission in Poly(Methyl Methacrylate) by Inner Shell Excitation

Nobuo UENO and Kenichiro TANAKA *(Hiroshima Univ.)*

The results of photon-stimulated ion desorption (PSID) from thin solid films of poly(methyl methacrylate) (PMMA) and corresponding polymers, poly(methyl acrylate) (PMA) and poly(methacrylic acid) (PMAA), owing to inner-shell excitation, are briefly reviewed. The results show that an enhancement of PSID takes place effectively upon electron excitation to a particular antibonding molecular orbital, indicating that the excitation to the antibonding state plays a major role in PSID enhancement. As a typical example, CH_3^+ desorption via oxygen 1s electron excitation was shown as a function of photon energy. By comparison of the photon energy dependences of PSID yields of CH_3^+ from the three polymers, it was found that the excitation of oxygen ls electron at OCH₃ to the cr* state localized at COCH₃ in PMMA results in the enhanced emission of CH_3^+ by bond scission at the side chain (0-CH₃), not at the main chain. The results indicate that there is a strong correlation between the sites of excitation and the following chemical-bond rupture. It is pointed out that monochromatic synchrotron radiation can be used as a "scalpel" to cut a chemical bond selectively in a molecular solid.

VI-L-5 Study of Solid Surfaces by Metastable Electron Emission Microscopy: Energy-Filtered Images and Local Electron Spectra at the Outermost Surface Layer of Silicon Oxide on Si(100)

Susumu YAMAMOTO *(Univ. Tokyo)*, **Shigeru MASUDA** *(Univ. Tokyo)*, **Hideyuki YASUFUKU** *(Chiba Univ.)*, **Nobuo UENO, Yoshiya HARADA** *(Chiba Univ.)*, **Takeo ICHINOKAWA** *(Waseda Univ.)*, **Makoto KATO** *(JEOL)* **and Yuji SAKAI** *(JEOL)*

We have observed images and local electron spectra of an oxide pattern on Si(100) using metastable electron emission microscopy (MEEM) recently developed at our laboratory. Low-energy electron microscopy (LEEM) was also used. For both MEEM and LEEM, the energy-filtered images were obtained for the first time. It was shown that MEEM gives the

information on the outermost surface layer selectively, while LEEM provides averaged information on several surface layers. The intensity of the band in the local electron spectrum of MEEM can be related to the distribution of the relevant orbitals exposed outside the surface, with which metastable atoms interact effectively. Thus, using energy-filtered MEEM, we can observe the map reflecting the distribution of individual orbltals at the outermost surface layer.

VI-L-6 Low-Energy Electron Transmission Spectroscopy of Thin Films of Chloroaluminum Phthalocyanine on MoS_2

Nobuo UENO, Yasushi AZUMA *(Chiba Univ.)*, **Takayuki YOKOTA** *(Chiba Univ.)*, **Masaru AOKI** *(Univ. Tokyo)*, **Koji K. OKUDAIRA** *(Chiba Univ.)* **and Yoshiya HARADA** *(Chiba Univ.)*

The growth of chloroaluminum phthalocyanine (CIAIPc) thin films on MoS_2 Surfaces was studied by low-energy electron transmission (LEET) spectroscopy. We observed that the as-grown monolayer, prepared by vacuum deposition, consists of islands of CIAIPc multilayers and the molecules spread over the substrate surface to form a uniform monolayer by heat treatment. Furthermore, we found that for heat-treated films the vacuum level of the sample system oscillates with increasing the film thickness from 0 to 2 monolayers. For the monolayer, the change of the vacuum level with respect to the substrate ($= \phi_{film} - \phi_{substrate}$) was positive, while for the doublelayer it was negative. These results indicate that in the monolayer the molecules lie flat with the Cl atoms protruding outside the film to form an electric dipole layer directing to the substrate and in the doublelayer the molecules in the outer layer are turned over with the Cl atoms protruding inside the film to compensate the dipole originating from the first monolayer. Furthermore the thickness independent characteristics of LEET spectra above the doublelayer suggest that thicker films consist of a stack of a double layer-like structures.

VI-L-7 Photon Stimulated Ion Desorption of Deuterated Polystyrene Thin Films Induced by Core Excitation

Kentaro FUJII *(Hiroshima Univ.)*, **Tetsuji SEKITANI** *(Hiroshima Univ.)*, **Kenichiro TANAKA** *(Hiroshima Univ.)*, **Shuuhei YAMAMOTO** *(Chiba Univ.)*, **Koji K. OKUDAIRA** *(Chiba Univ.)*, **Yoshiya HARADA** *(Chiba Univ.)* **and Nobuo UENO**

Photon stimulated ion desorption (PSID) of thin films of selectively deuterated polystyrene ($[-CD_2-CD-(C_6H_5)-]_n$, $[-CH_2-CH(C_6D_5)-]_n$ and $[-CD_2-CD(C_6D_5)-]_n$) have been investigated to reveal the mechanism of surface photochemical reactions following core excitation. Desorbing ions were measured using the

time-of-flight mass spectrometer (TOF-MS) combined with a pulsed synchrotron radiation. From the total electron yield spectrum and partial ion yield spectrum of each sample, it is concluded that D^+ ions are mainly desorbed from the phenyl group and the yield of D^+ is enhanced at the C-D* resonance. From the ion kinetic energy distribution obtained from analysis of the TOF spectrum, the ions desorbed from the phenyl group have different kinetic energy distribution. The results are discussed in connection with the mechanism of PSID.

VI-L-8 Characterization of Self-Assembled Monolayer of Thiophenol on Gold by Penning Ionization Electron Spectroscopy

Abuduaini ABDUREYIM *(Chiba Univ.)*, **Satoshi KERA** *(Chiba Univ.)*, **Masaru AOKI** *(Univ. Tokyo.)*, **Koji K. OKUDAIRA** *(Chiba Univ.)*, **Nobuo UENO** **and Yoshiya HARADA** *(Chiba Univ.)*

The molecular orientation in self-assembled monolayers (SAMs) of thiophenol chemisorbed on polycrystalline gold from aqueous solutions has been investigated by Penning ionization electron spectroscopy (PIES) and ultraviolet photoelectron spectroscopy (UPS). The analysis of the relative band intensity of the Penning spectrum indicates that the phenyl ring in phenyl thiolate stands perpendicular to the substrate plane at room temperature. Upon heating the phenyl ring becomes tilted in the layer.

VI-L-9 High-Resolution Electron Energy Loss Spectroscopy of Chloroalminum Phthalo-cyanine Ultrathin Films

Yasushi AZUMA *(Chiba Univ.)*, **Takayuki YOKOTA** *(Chiba Univ.)*, **Satoshi KERA** *(Chiba Univ.)*, **Masaru AOKI** *(Univ. Tokyo)*, **Koji K. OKUDAIRA** *(Chiba Univ.)*, **Yoshiya HARADA** *(Chiba Univ.)* **and Nobuo UENO**

High-resolution electron energy loss spectra (HREELS) were measured for ultrathin films of chloroaluminum phthalo-cyanine (CIAIPc) deposited on a cleaved HOPG surface in order to investigate the molecular orientation and its thickness dependence. It was found that for the monolayer film CIAIPc molecules lie flat on the HOPG surface without heat treatment. With increase in the film thickness, the molecules become oriented at a tilt. The result show a marked difference from the orientation of CIAIPc molecules on MoS_2, where the molecules lie tilt on MoS_2 in the as-grown monolayer.

VI-L-10 Angle-Resolved UPS Study and Simulation with IAC Approximation for Oriented Monolayer of Tetratetracontane (*n*-$C_{44}H_{90}$) on Cu (100)

Daisuke YOSHIMURA *(Nagoya Univ.)*, **Hisao ISHII** *(Nagoya Univ.)*, **Yuhiko OUCHI (Nagoya Univ.), Eisuke ITO** *(Nagoya Univ.)*, **Takayuki MIYAMAE Shinji HASEGAWA, Nobuo UENO and Kazuhiko SEKI** *(Nagoya Univ.)*

The electronic structure and orientation of tetratetracontane (*n*-$C_{44}H_{90}$, TTC) monolayer film on Cu(100) were studied by angle-resolved UPS (ARUPS). We observed a 2×1 LEED pattern at room temperature. This indicates that the TTC molecule lies on the Cu(100) surface with its chain axis parallel to the Cu(110) direction. The application of the dipole selection rules to normal emission spectrum revealed that the C-C-C plane of TTC is parallel to the surface (flat-on orientation). We also examined the dependence of the photoemission spectra on the take off angle. The simulated spectra for flat-on orientation based on independent atomic center (IAC) approximation combined with *ab initio* MO calculations are in good agreement with the observed spectra. These results verify the deduced molecular orientation and demonstrate the reliability of theoretical simulation with IAC approximation.

VI-M Formation of Nanometer-Scale InAs Island on GaP (001) Substrate

For three-dimensional confinement of electrons and holes, new physical phenomena and improvement of optoelectronic devices, such as extremely sharp emission line, phonon relaxation bottleneck, and temperature independent threshold current density for lazing, have been predicted. InAs quantum dots on GaP are very attractive since the band-offset in the conduction band is expected to be as large as 1 eV. Furthermore, there is a large mismatch of 11% in lattice constants between InAs and GaP, which modifies their energy band structures.

VI-M-1 Nanometer-Scale InAs Islands Grown on GaP (001) by Organometallic Vapor Phase Epitaxy

Youichi NONOGAKI, Tadashi IGUCHI *(Nagoya Univ.)*, **Shingo FUCHI** *(Nagoya Univ.)*, **Yasufumi FUJIWARA** *(Nagoya Univ.)*, **Yoshikazu TAKEDA** *(Nagoya Univ.)*

We have successfully grown nanometer-scale InAs islands on GaP (001) by low-pressure organometallic vapor phase epitaxy (LP-OMVPE). Effects of substrate temperature and InAs deposition rate on the shape, size and areal density of InAs islands were investigated by *ex-situ* atomic force microscope (AFM) and high-energy electron diffraction (HEED). The AFM observations showed that the island size decreased with the substrate temperature while the areal density increased, indicating that migration play a role on island formation. The HEED patterns provided significant result that the island grown at high temperature (650°C) consisted of a few grains, while the island grown at low temperatures (550 and 500°C) was single crystalline.

VI-M-2 Effects of Post Annealing on Self-organized InAs Islands Grown on (001) GaP by Organometallic Vapor Phase Epitaxy

Shingo FUCHI *(Nagoya Univ.)*, **Youichi NONOGAKI, Tadashi IGUCHI** *(Nagoya Univ.)*, **Hiromitsu MORIYA** *(Nagoya Univ.)*, **Yasufumi FUJIWARA** *(Nagoya Univ.)*, **Yoshikazu TAKEDA** *(Nagoya Univ.)*

Using atomic force microscopy (AFM) and transmission electron microscopy (TEM), we have investigated effects of post annealing on self-organized InAs islands grown on (001) GaP by low-pressure organometallic vapor phase epitaxy (LP-OMVPE). The morphology of InAs islands without the cap layer depended strongly on the growth temperature, which was related to migration of InAs adsorbed on GaP. Subjected to the annealing at temperatures higher than the growth temperature, the small islands coalesced each other to form larger islands. The resultant morphology was quite similar to that of the samples grown at the annealing temperature. Cross-sectional TEM observation was carried out on the buried InAs islands. Almost relaxed InAs islands buried by the GaP cap layer with stacking faults were clearly observed. The size and density of the buried InAs islands were similar to those in the samples post-annealed at the growth temperature of the GaP cap layer, suggesting that the change on the InAs islands was induced during the increase in the substrate temperature for the GaP cap-layer growth. These results indicated that the growth temperature for the GaP cap layer played an important role in fabricating the sandwich structures with frozen small InAs islands.

VI-N Desorption Induced by Electronic Transitions (DIET) from Cryogenic Surfaces

Desorption processes of particles from cryogenic surfaces are studied using synchrotron radiation in soft X-ray and vacuum ultraviolet region. As a result of decay processes after an electronic excitation of surface layers by synchrotron radiation, various kinds of particles are released from the surface. For example, solid rare gases have particular excitation channels for the desorption of electronically excited neutral particles that are pronounced at the creation energy region of exciton. Experiments are performed at BL2B1 and BL5B of UVSOR. At BL5B the energy range is mainly on valence exciton region, and excited neutral particles and photons emitted during the desorption process are measured. On the other hand, SR in core excitation region is used at BL2B1, and desorbed ions are measured in a coincidence with Auger electron from molecules which produce fragment ions.

VI-N-1 Absolute Desorption Yield of Metastable Atoms from the Surface of Solid Rare Gases Induced by Exiton Creation

Takato HIRAYAMA *(Gakushuin Univ.)*, **Akira HAYAMA** *(Gakushuin Univ.)*, **Toshihiro KOIKE** *(Gakushuin Univ.)*, **Takafumi KUNINOBU** *(Gakushuin Univ.)*, **Ichiro ARAKAWA** *(Gakushuin Univ.)*, **Koichiro MITSUKE, Makoto SAKURAI and E. V. SAVCHENKO** *(B. Verkin Inst. for Low Temp. Phys. and Eng.)*

Absolute yields of the metastable excited atoms desorbed from the surfaces of solid Ne and Ar by the creation of surface and bulk excitons have been measured using monochromatized synchrotron radiation as a selective excitation source. We have obtained the absolute yields of $(2.3\pm0.7) \times 10^{-3}$, $(1.4\pm0.4) \times 10^{-3}$, and $(7.8\pm2.3) \times 10^{-4}$ (atoms/photon) at the excitation of S1, B1 and S' exciton for Ne, respectively, and 1×10^{-5} (atoms/photon) at S1 excitation for Ar. The probability for metastable atom desorption is found to be about 2 to 10% at the excitation of S1 exciton on the surface of solid Ne.

VI-N-2 Long Lifetime Emission of the Excited Species Ejected from the Surface of Solid Ne

E. V. SAVCHENKO *(B. Verkin Inst. for Low Temp. Phys.)*, **Takato HIRAYAMA** *(Gakushuin Univ.)*, **Akira HAYAMA** *(Gakushuin Univ.)*, **Toshihiro KOIKE** *(Gakushuin Univ.)*, **Takafumi KUNINOBU** *(Gakushuin Univ.)*, **Ichiro ARAKAWA** *(Gakushuin Univ.)*, **Koichiro MITSUKE and Makoto SAKURAI**

Desorption of long-lived neutral particles from solid Ne is studied using selective photoexcitation and time of flight (TOF) technique. The luminescence due to direct light from the sample surface is blocked by rotating the sample. Two new prominent features are revealed in the TOF spectra measured at a special geometry: a prominent long tail and a maximum at the delay time of ~ 0.5 ms. From the analysis of the excitation spectra recorded by the time window technique and the TOF spectra at selective excitation it is assumed that the new features are closely related to Ne_2^* excimer desorption. Analysis of probable mechanisms of the long lifetime emission is presented.

VI-O Structure and Vibrational Spectra of Molecules Physisorbed on Metal Surfaces

Molecular layers physisorbed on metal surfaces at low temperature show specific structures which depend on the interaction between molecules and substrate, and vibrational spectra for physisorbed molecules reveal the details of the interaction. We use dynamical analysis of low-energy electron diffraction (LEED) to investigate the structure of adsorbed layers, and high-resolution electron energy loss spectroscopy has been utilized for vibrational spectroscopy for adsorbed molecules. As a complemental method for vibrational spectroscopy of surfaces, infrared reflection absorption spectroscopy will be combined with our experimental system. A new cryogenic sample holder for surface vibrational spectroscopy is also under development in order to provide a substrate at less than 4.2K.

VI-O-1 Upgraded Infrared Beamline BL6A1 at UVSOR

Makoto SAKURAI, Hidekazu OKAMURA *(Kobe Univ.)*, **Katsumi WATANABE** *(Kobe Univ.)*, **Takao NANBA** *(Kobe Univ.)*, **Shin-ichi KIMURA and Masao KAMADA**

BL6A1, a far-infrared (FIR) beamline at UVSOR originally built in 1986, has been upgraded recently. The upgrade included the introduction of a second FT-IR spectrometer, and now it is possible to cover the entire FIR-IR range (3 cm^{-1} to 10000 cm^{-1}) in one sequence of measurements, without having to open the sample chamber; the beamline has become a more convenient and powerful experimental station than before. The upgrade is also expected to enable such experiments as IR studies of molecules adsorbed on the solid surfaces, and time-resolved IR spectroscopies.

VI-O-2 Development of High Sensitivity EELS

Makoto SAKURAI

Electron energy loss spectroscopy (EELS) is a powerful tool for the structural analysis of molecules adsorbed on a solid surface. However, since ordinary EELS system uses a single channel electron analyzer, the measurement time for one spectrum usually amount to several minutes. This has been a disadvantage of EELS for real time analysis of surface reaction. We develop a new electron analyzer for EELS. The analyzer is a simulated hemispherical analyzer with a position sensitive detector. The components are made of aluminum (YH75), and mean radius of the deflector is 104 mm. The detector has CR chain type anode, and the signal is stored to a histogramming memory via posision analyzer. The spectrum can be measured as frequent as every 100 μs. This feature make it possible to perform a time resolved measurement of repetitive reaction processes.

VI-O-3 Electronic Structure of a Pt(111)-Ge Surface Alloy and Adsorbed CO

Katsuyuki FUKUTANI *(IIS Univ. Tokyo)*, **Tamerlan MAGKOEV** *(IIS Univ. Tokyo)*, **Yoshimasa MURATA** *(Univ. Electro-Communications)*, **Masuaki MATSUMOTO, Taizou KAWAUCHI** *(IIS Univ. Tokyo)*, **Tamotsu MAGOME** *(IIS Univ. Tokyo)*, **Yasuhisa TEZUKA** *(ISSP Univ. Tokyo)*, **Shik SHIN** *(ISSP Univ. Tokyo)*

Angle-integrated photoemission spectra are observed for Pt(111) and a Pt(111)-Ge surface alloy. The spectra for Pt(111)-Ge show d-band filling compared with those for Pt(111). Although the chemisorption energy of CO is noticeably reduced by alloy formation, the binding energies of the occupied levels for adsorbed CO are almost the same as those on pure Pt(111). The results are discussed by the d band filling due to s-d hybridization of Ge s electrons and the Pt d band and by two-level hybridization of the 5 and 2 states with the modified d band.

VI-O-4 LEED and STM Measurement of NO /Pt(111) at Low Temperature

Masuaki MATSUMOTO, Toshiyuki YAMADA *(Tsukuba Univ., CREST)*, **Natsuo TATSUMI** *(IIS Univ. Tokyo)*, **Tadashi ITOYAMA** *(IIS Univ. Tokyo)*, **Kouji MIYAKE** *(Tsukuba Univ., CREST)*, **Kenji HATA** *(Tsukuba Univ., CREST)*, **Hidemi SHIGEKAWA** *(Tsukuba Univ., CREST)*, **Katsuyuki FUKUTANI** *(IIS Univ. Tokyo)* **and Tatsuo OKANO** *(IIS Univ. Tokyo)*

The chemisorption of nitric oxide on Pt(111) at low temperature has been studied by electron energy loss spectroscopy (EELS), infrared absorption spectroscopy (IRAS) and low energy electron diffraction (LEED). The vibrational spectroscopy showed that N-O stretching frequency is 1490 cm^{-1} at low coverage (< 0.5 L) and 1710 cm^{-1} at high coverage (> 0.5 L). At high coverage, 2×2 LEED pattern was observed and its structure was attributed to the fcc hollow site by LEED dynamic theory. But there is no reasonable account for the difference of the N-O stretching frequency between low and high coverage regions and the structure is controversial yet. We measured the LEED I-V curves and STM images of NO/Pt(111) surface at several temperature and coverage conditions. At 175K, diffuse 2×2 LEED pattern could be seen even at low dosage (0.05L) and the I-V curve was the same as that at high dosage (1L). This indicates that (2×2)-NO islands grow with coverage increase but the local structure does not change at this temperature region.